Electrical Power and Energy Systems 153 (2023) 109310

Contents lists available at ScienceDirect

International Journal of Electrical Power and Energy Systems

journal homepage: www.elsevier.com/locate/ijepes

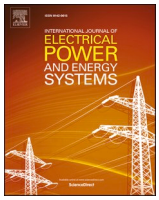

A novel resilience assessment for active distribution networks including a DER voltage regulation scheme considering windstorms

Alexandre Serrano-Fontova [a,*], Zhiyu Liao [a], Haiyu Li [a], Campbell Booth [b]

[a] School of Electrical and Electronic Engineering, The University of Manchester, Manchester M60 1QD, UK
[b] Department of Electronic and Electrical Engineering, The University of Strathclyde, Glasgow G1 1XW, UK

ARTICLE INFO

Keywords:
Resilience
Active Distribution networks (ADNs)
Distributed generation (DG)

ABSTRACT

Increasing incidences of extreme weather events pose significant challenges to the electrical grids in terms of the ability to withstand those high-impact eventualities. This paper proposes a resilience assessment framework for net-zero active distribution networks (ADNs) to tackle the impacts of extreme windstorms where only renewable energy resources (RESs) and battery energy storage systems (BESSs) are considered. To accurately capture the influence of windstorms on the grid, a detailed spatiotemporal representation of grid system assets and their exposure to the wind has been implemented. The suggested day-ahead resilience assessment is based on a three-stage approach. The first stage computes the probabilities of failure of each line and determines the most vulnerable ones. The second stage obtains the optimal grid configuration based on the outcomes of the first stage given the available non-dispatchable RESs and commits the available resources in each island to minimize the loss of load during the windstorm. If such a value is still larger than zero after the second stage, a novel voltage regulation scheme is applied in the third stage, taking advantage of the RESs and BESSs in each island. The proposed resilience assessment has been evaluated using the IEEE 33-bus test system with the meteorological data retrieved from an actual windstorm event occurred in the UK on the 20th of February. The outcomes of this paper underscore that a significant reduction in load shedding during such extreme events can be achieved, thus having a notable enhancement to the overall resilience of the system. Finally, the performance of this approach is compared with other resilience-oriented methods for windstorms, where the benefits of using the scheme reported in this paper are highlighted and quantified.

1. Introduction

During recent years, extreme weather-related events have notably risen and, unfortunately, become more frequent. It can be stated that this is related to climate change, as outlined in the latest report released by the intergovernmental panel on climate change (IPCC) [1]. Natural hazards are processes that serve as triggers for natural disasters. According to [2], natural hazards can be organized into six categories. However, by disregarding biological and extraterrestrial hazards, four categories are obtained. Firstly, geological hazards relate to the movement of solid earth, including earthquakes and volcanic activity. Secondly, hydrological hazards relate to the movement of water and essentially entail floods, landslides, and wave action, whereas the third group purely fall within the meteorological events such as storms, extreme temperatures, and fog. In the last instance, the climatological events have been directly related by scientists to greenhouse effects, including droughts and wildfires.

The electrical networks are highly affected by such eventualities, where the security of supply is typically one of the major concerns [3]. Focusing solely on windstorms, several events have been reported to be severely damaging and causing large disruptions across the world, as can be seen in the comprehensive report carried out by [4], where some indexes are proposed. As an example, recent windstorms named Dudley, Eunice and Franklin hit the UK in 2021/2022, causing an estimated economic loss of £497 m and approximately 1.4 million households were left without power [5]. In the US, hurricanes Harvey, Irma, and Maria caused an estimated total economic loss of around $202 billion [6]. In February 2021, the windstorm in Texas led to large-scale generator outages and load shedding of up to 25GW (33 % of total load), where 4.5 million customers were left unserved during the most serious period (February 15th ~ 16th) [7].

At the COP meeting in 2022, there was a commonly stated goal relating to achieving a net-zero emissions target whilst guaranteeing a

* Corresponding author.
E-mail address: alexandre.serrano-fontova@manchester.ac.uk (A. Serrano-Fontova).

https://doi.org/10.1016/j.ijepes.2023.109310
Received 29 November 2022; Received in revised form 8 March 2023; Accepted 11 June 2023
Available online 21 June 2023

Nomenclature

Abbreviation

RES	Renewable energy resources
DG	Distributed generation
MG	Microgrid
DSO/TSO	Distribution/Transmission operator
MILP	Mixed-integer linear program
OHL	Overhead line
ND	Non-dispatchable
BESS	Battery Energy storage system
M	A large number
P	Active Power
Q	Reactive Power
S	Apparent Power
$V^{\max}/V^{\min}$	Max./Min. Voltage magnitude
FC	Fragility curve

Indices/Sets

$_i$	Index for buses
$_{ij}$	Indices for branches
$_t$	Index for time
$_s$	Index for buses on each island
$_k$	Index for poles
Ω_L	Set of lines
Ω_P	Set of poles
Ω_A	Set of pole ages
Ω_B	Set of buses
Ω_{type}	Set of pole types
Ω_{class}	Set of wood pole classes
Ω_{ij}^{P}	Set of poles in each of *ijth* line
$\Omega_{s,t}$	Set of buses in the *sth* island
$\Omega_{s,t}^{root}$	Set of island roots at time *t*
Ω^{DER}	Set of non-dispatchable DERs
Ω^{ESS}	Set of BESSs
$\Omega_{s,t}^{ESS}$	Set of BESSs in the *sth* island
$\Omega_{s,t}^{DER}$	Set of DERs in the *sth* island
$\Omega_{ij,t}^{P}$	Set of failure probabilities for each *ijth* line at time *t*
Ω_{FC}	Set of Fragility curves
$\Omega_{ij,t}^{V}$	Set of vulnerable lines at time *t*
$\Omega_{parent,i}$	Set of parent buses of the *i*th bus
$\Omega_{children,i}$	Set of children buses of the *i*th bus

Parameters

r_{ij},x_{ij}	Resistance/reactance of the *ijth line*
P_i^{peak}	Peak power of a PV unit at the *ith* bus
T^{sd}	PV Standard Temperature [deg.]
T^{amb}	Ambient Temperature [deg.]
I_t^r	Net solar irradiance at each time *t*
I_t^{sd}	Standard solar irradiance
T_t^c	PV Cell Temperature at time *t*
P_i^{peak}	Peak power of a PV unit at the *ith* bus
αpv	Coefficient used in PV modelling
p_{thr}	Vulnerability Threshold
$\Delta V^{\max}$	Maximum voltage drop
V_i^o	Rated Voltage magnitude of the *i*th bus
V_o	Rated voltage magnitude
u_t	Wind gust at each time *t* [m/s]
C_i^{LF}	Cost of Flexibility [£/kW]
$K_{i,Z}$, $K_{i,I}$, $K_{i,P}$	Share of each type of load model for active power
C_i^{LS}	Cost of Load shedding [£/kW]
N_{ij}	Number of lines in the test system
T	Number of time periods
N_p	Number of poles in the test system
C_i^{SU}	Cost of the energy from the main grid [£/kWh]
N_{ij}^{Poles}	Number of poles in each *ij* line

Variables

$N_t^{Islands}$	N° of islands at each time *t*
$N_{s,t}^{ESS}$	N° of BESSs on the *sth* island
$N_{s,t}^{DER}$	N° of DERs on the *sth* island
$\alpha_{ij,t}$	Binary variable for the *ijth* line out of service
$P_{k,ij,t}$	Failure probabilities of poles within the *ij*th line at time *t*
$P_{k,t}$	Failure probabilities of poles at time *t*
$P_{ij,t}^{L}$	Probability of failure of the *kth* line
$P_{ij,t}^{B}$	Failure probability of line *ij* due to wire break
$P_{ij,t}^{P}$	Failure probability of line *ij* due to pole collapse
$P_{i,t}^{SU}$	Substation Active power
$Q_{i,t}^{SU}$	Substation Reactive power
$P_{i,t}^{SUMax}$	Max. Substation Active power
$Q_{i,t}^{SUMax}$	Max. Substation Reactive power
$P_{i,t}^{DER}$	Active power of DER in the *i*th bus
$Q_{i,t}^{DER}$	Reactive power of DER in the *i*th bus
$P_{i,t}^{DER\max}$	Max. Active power of DER in the *i*th bus
$Q_{i,t}^{DER\max}$	Max. Reactive power of DER in the *i*th bus
$P_{i,t}^{FL}$	Active power used as flexibility in the *i*th bus
$Q_{i,t}^{FL}$	Reactive power used as flexibility in the *i*th bus
$P_{i,t}^{FL\max}$	Flexibility Max. Active power in the *i*th bus
$Q_{i,t}^{FL\max}$	Flexibility Max. Reactive power in the *i*th bus
$P_{i,t}^{L}$	Load active power in the *i*th bus
$Q_{i,t}^{L}$	Load Reactive power in the *i*th bus
$P_{i,t}^{o}$	Active power load at V_i^o in the *i*th bus
$Q_{i,t}^{o}$	Reactive power load at V_i^o in the *i*th bus
$P_{i,t}^{ESSD}$	P_D of the BESS at the *i*th bus
$P_{i,t}^{ESSC}$	P_C of the BESS at the *i*th bus
$P_i^{ESSDmax}$	Max. P_D of the storage unit at the *i*th bus
$P_i^{ESSCmin}$	Min P_C of the storage unit at the *i*th bus
$SoC_{i,t}$	State-of-charge of the BESS at the *i*th bus
$P_{i,t}^{W}$	Wind-based DER Active power at the *i*th bus
$P_{i,t}^{PV}$	PV-based DER Active power at the *i*th bus
$P_{i,t}^{LS}$	Load shedding in the 2nd stage (Active power)
$Q_{i,t}^{LS}$	Load shedding in the 2nd stage (Reactive power)
$\Delta P_{s,t}^{REG}$	Active power used for regulation in each *sth* island
$\Delta V_{s,t}^{REG}$	Max. Voltage regulation in the *sth* island
$\Delta P_{s,t}^{REG\max}$	Max. Active power regulation in the *sth* island
$\Delta P_{s,t}^{REG}$	Active power regulation in the *sth* island
$\Delta V_{s,t}$	Max. Voltage drop in the *sth* island
$V_{s,t}$	Root Voltage set-point in the *sth* island
$\Delta P_{i,t}^{LS}$	Load shedding difference
$P_{ij,t}$	Active power flow along the *ijth* line
$Q_{ij,t}$	Reactive power flow along the *ijth* line
$P_{ij,t}^{\max}$	Max. active power flow along the *ijth* line
$Q_{ij,t}^{\max}$	Max. reactive power flow along the *ijth* line
$S_{ij,t}$	Apparent power flow along the *ijth* line
$S_{ij,t}^{\max}$	Max. Apparent power flow along the *ijth* line
$V_{i,t}$	Voltage magnitude of the *i*th bus
$K_{i,z}'$,$K_{i,I}'$, $K_{i,P}'$	Share of each type of load model for reactive power

secure and resilient energy system [8]. In line with this agreement, the UK government has set a roadmap to become a net-zero country by 2050 [9]. Even though RESSs offer many advantages, the inherent intermittency and technical issues associated with the energy conversion process pose a challenge to system operators [10]. To that end, fostering the development of new techniques to enhance resilience seems to be crucial. In Refs. [3,11–13], resilience has been defined as the ability to anticipate, absorb, and recover from the effects of hazardous events in a timely and efficient manner.

The UK Energy Research Centre (UKERC) defined the term resilience regarding energy systems as the capacity to tolerate disturbances, including the ability to recover speedily from shocks and continue to deliver affordable energy services to customers [14]. In this context, the United Nations – International Strategy for Disaster Reduction (ISDR) defined resilience as a degree of a system's adaptability to maintain its functionalities and cope with hazards by organising and learning from past disasters, see [15].

1.1. Literature review

As described in the previous Section, until today, it appears to be little consensus, if any, among the scientific community when it comes to resilience classification in power systems. A summary of the principal references published so far is provided below.

In [16], the authors opted for categorising the resilience assessments into; performance-based, implementation-based, temporality-based, interdependent system and event-based. On the other hand, according to [17], resilience assessments can be distinguished into two major types: structural (i.e., planning) and operational. The latter one includes three types of actions according to the event timeline, thus being evaluated *before*, *during* and *after* the event. When the resilience evaluation is carried out before the event, it entails all preventive measures for preparedness and readiness regarding weather-related or human threats. In addition to that, if the assessments are aimed at tackling the outage effects throughout the event, these are known as *corrective strategies*. In this vein, every system resource should mitigate the effects of such events as part of a real-time scheme (e.g., protective coordination, frequency control, fast generation response, etc.). Finally, in the aftermath of the event, restorative endeavours are crucial to reach the pre-event status. The post-contingency actions are known as *restorative strategies* and can be divided into several stages according to the adopted scheme.

Authors in [18] have comprehensively recalled the role that MGs can play towards resilience, wherein the articles are divided into *investment planning*, *pre-event preparation*, and *post-event operation* according to their operational features, therefore being in accord with the distinction made in [17].

Based on the previous distinction, the resilience assessments have been further classified into two main typologies named (i) *Planning and investment* and (ii) *operational*, as illustrated in subsections 1.1.1 and 1.1.2, respectively.

1.1.1. Planning and investment resilience assessments

Resilience studies focused on the long run, where the main goal is how to optimally invest revenues and maximising the resilience of the grid against major contingencies, are classified as planning and investment assessments [19–22]. These studies can be performed considering stochastic techniques to determine the optimal actions to harden the grid considering a wide range of contingencies, including severe natural disasters. In [17], a planning model has been presented which proposed a resilience strategy using backup distributed generations (DGs), ties lines and line hardening under natural disaster conditions such as earthquakes and floods. The distribution system planning considers the minimisation of the daily investment, operation, and resiliency (i.e., both repair and load shedding) costs as objective functions subject to many constraints. In [18], however, a stochastic two-stage optimisation problem to compute a new resilience index based on the social welfare concept to cope with hurricanes is considered. The proposed new resilience index is optimised with effective strategies, including upgrading distribution poles, DER allocation with different capacities and distribution system automation.

The objective of [19] is to proactively allocate and mobilise the available resources to enable a quick response to repair and restore the system after an event to reduce the expected incurred costs. To fulfil such achievement, the optimisation problem is modelled as a stochastic integer program with complete recourse where the repair time and failure state of the assets are modelled as random variables in the second stage. This study has evaluated three main scenarios, thus obtaining the optimal grid reconfiguration and allocating backup resources.

From the investor point of view, the authors in [20] proposed a trilevel investment planning for distribution networks with large penetration of DER. In this regard, this study is aimed at maximising the net present value of the DERs in distribution networks, where a robust optimisation is utilised to cope with physical and financial data uncertainty in load demand, DERs output, and energy prices. The outstanding results obtained in such a study endorse the suitability of this strategy to allocate DERs efficiently in distribution networks.

1.1.2. Operational resilience assessments

This Section aims at reviewing the main features of the operational resilience assessments. As briefly introduced before, the operational studies can be classified according to the instant in time when they focus the action (i.e., *before*, *during* or *after* the event time occurrence). It is worth highlighting that some articles have proposed joint schemes combining preventive and corrective measures, thus accounting for the *before* and *during*.

As a preventive measure, a vital step lies in establishing the metrics to measure resiliency and therefore computing the degree of risk that the electrical grid faces. Although there is not yet unanimous consent toward resilience metrics standards, valuable contributions have been reported in [23–27]. In [23], the primary concept of a resilience trapezoid to display the resilience of the grid has been replaced by a novel multi-stage process. Concretely, it considers all the phases that critical infrastructure, including power systems, might reside in during an event and the transition between these states. A time-dependent operational and infrastructure resilience metrics based on different indicators are proposed in this work to quantify this multi-phase resilience trapezoid according to the pre-event, during-event actions and system recovery. In this direction, [24] recalls the stages of a resilience assessment and, for the first time, proposes the required metrics for the so-called multi-stage recovery process (i.e., ΦΛΕΠ Metrics). In this methodology, each Greek letter stands for a particular stage of the assessment (e.g., $\Phi\Lambda$ belongs to disturbance progress, E represents the effectiveness when dealing with the contingency, whereas Π measures how fast it recovers). Once such an index is obtained, the resilience of the network is quantified, and further actions can be taken. Within the operational risk evaluations, the authors in [25] presented both the implementation of defensive islanding to deal with the effects and windstorms and the development of a severity risk index. Crucially, such an index is used to determine the application of defensive islanding, which considers the current network topology and the branches at higher risk of tripping due to the windstorm. In this study, real wind profiles and several scenarios have been taken into consideration.

To grapple with the effects of a windstorm and reduce the load shedding throughout these events, [28] developed resilience-oriented strategies to properly set out the DERs scheduling in distribution networks. In [29], the IEEE 33-bus test system has been divided into three areas to capture the dynamic behaviours of these disasters. Additionally, the unavailability uncertainties of *N-K* contingencies are considered along with the forecast uncertainties of load demand, wind power, and solar power. Concomitantly, the authors in [30] addressed the problem at hand by performing a reconfiguration, generation re-schedule, conservation voltage regulation, optimal parameter settings of droop-

controlled units, demand-side resources, and backup generation capacity. A vulnerability index is defined to assess the effectiveness of the proposed proactive technique.

In line with the previous two studies, [31] have delved into the operational assessment yet put special emphasis on the grid reconfiguration. The methodology has exhibited a high performance to enhance the distribution system resilience, especially for low to moderate penetration levels of DERs. The strategy includes post-fault reconfiguration and optimal scheduling of dispatchable or non-dispatchable DERs. In addition, a recent article covered the effects that a pandemic situation like COVID-19 can cause on the electrical networks' resiliency [32].

Thirdly, the research in [33] exemplifies a resilience assessment entirely focused on restoration. A coordinated TSO/DSOs strategy has been analysed to recover the system in a reliable manner even though these two systems are commonly operated separately. The outcomes of such a study revealed that the integrated transmission and distribution systems restoration (ITDSR) developed in this paper proved successful in jointly (i.e., TSO/DSO) restoring the system after the contingency has occurred. The presented ADMM-ITDSR model includes a convex ac power flow model and three-phase unbalanced branch flow model and coordinates the assets in both networks, including a high share of DERs.

1.2. Contribution and paper structure

Based on the previous state-of-the-art review, it is seen that implementing advanced schemes and tools to address the undesired effects of windstorms in distribution networks is of utmost importance. The contribution towards distribution network resilience enhancement covered in this paper can be summarised as follows:

1. Some resilience assessments (e.g., see [28]) have neglected pole deterioration and uniquely considered one type of pole, thus having a great impact on the outcomes. In this paper, nevertheless, a detailed casuistry has been considered to properly represent deterioration and its effects on failure probabilities. In particular, two types of poles (i.e., wood and steel), classes (e.g., Class 3 and Class 5), ages, and leaned poles have been modelled. Thence, the spatiotemporal approach accounted for in this paper provides an accurate enough representation to capture the system susceptibility. The implications of neglecting ages and types of poles in resilience assessments during windstorms are illustrated in Section 5.
2. Ref. [30,34–36] have taken advantage of dispatchable DERs as backup generators, which are useful resources to rely on when using non-dispatchable DERs such as solar and wind to restore the system. Even though highly efficient engines feed these dispatchable units, they use fossil fuels as the main source (e.g., natural gas). In the present approach, a net-zero carbon scenario is deemed with PV, wind power units and BESSs. According to [30,37], the PV profile is around 30 percent of the rated value during these contingencies. Therefore, the maximum PV radiation modelled in [28,29] for windstorms could lead to unrealistic scenarios. This paper has considered the solar irradiation and wind profile extracted from a real occurred windstorm in the UK. Additionally, it is seen that over the severest part of the storms, the gusts are above the cut-off wind speed, causing the disconnection of the wind turbines. Consequently, dealing with such extreme scenarios without relying on fossil fuel-based backup generators and/or microturbines becomes a challenge, which has been addressed in this article.
3. A three-stage process is considered where the first one essentially focuses on determining the vulnerable lines as the windstorm unfolds, given the spatiotemporal representation detailed in 1). Subsequently, the second stage lies in solving an optimisation problem with multiple constraints to obtain the grid configuration and feasible islands, the expected load shedding, the required flexibility and committing the BESSs. After that, the third stage determines the amount of load shedding (if any) that can be reduced by considering a novel voltage regulation scheme implemented using the DERs and BESSs on each island. This scheme relies on the nature of the DER (i.e., electronically interfaced). As the main principle, it uses the voltage drop obtained in each island in the second stage to determine the maximum amount of power that can be restored by using this scheme without violating the voltage constraints considered in the optimization problem.

The rest of the paper is organised as follows; Section 2 details the models considered to compute the failure probabilities of the test system components. Section 3 provides an in-depth explanation of the proposed resilience approach. The performance of the suggested technique is then assessed and thoroughly discussed under numerous case studies in Section 4. Section 5 compares the performance of the proposed method with the existing resilience-oriented assessments. Finally, Section 6 summarises the conclusions of this work.

2. Modelling the fragility of the system

In this subsection, the fragility of the test system components is modelled. Since this article has chosen the IEEE 33-bus system as a benchmark to test the effects of windstorms, poles and wires of overhead lines are the only assets exposed to such an event. In the present study, a total length of 2 km has been considered in each line with a span of 100 m between poles, then giving a total number of 640 poles.

Realistically, distribution networks are composed of aged poles wherein their reliability is being undermined in the curse of time [38]. In this sense, to accurately capture the effects of such deterioration over time, the authors have decided to implement a lognormal distribution with μ and σ of 3.44 and 0.2, respectively, having then ages normally distributed around 30-year-old poles.

As has been reported in Refs. [38–42,56], slight variations are observed in terms of robustness when different types of wood poles are subject to strong winds, particularly for those long-aged. Both the American national standards institute (ANSI) and the National electric safety code (NESC) outline the guidelines to be followed when designing and deploying wood poles in distribution networks. In addition to the studies on wood poles, other authors have explored the wind-fragility of both concrete and steel poles. In the proposed assessment, however, concrete poles were not included as steel and concrete proved to possess similar performance. Therefore, steel and wood poles (i.e., Class 3, Class 5, and class 5 with leaning angle) are those eventually chosen in the proposed system modelling. The fragility curves for steel poles can be found in [43], wood poles in [38], and the probability of failure of Class 5 bent poles in [44], respectively. Even though in the latter study, several leaning angle degrees have been scrutinised (e.g., 0/10/20/30 deg.), only 20 degrees leaned poles are used in our test system.

Since the fragility curves are based on a particular age range, the poles generated with the lognormal function have been regrouped into sets of ages (i.e., 10/20/30/40/50/60/70/80-years-old and 0/20/40/60-years-old for wood and steel poles, respectively).

Given that a real distribution network can be composed of underground and overhead lines (OVLs) [31], the network object of study has been divided according to the percentages listed in Table 1. In

Table 1
Data of the considered poles in this test system.

Poles and lines	N° of Poles	Fragility curves *(Ref.)*	Share of each Pole type(%)
OHL (Wood-C3)	192	[38]	30
OHL (Wood-C5)	152	[38]	23.75
OHL (Wood-C5LA*)	44	[44]	6.25
OHL (Steel)	192	[42]	30
Underground	64	–	10

* LA = Leaning angle.

accordance with the previous assertions, the probabilities of failure of each *ij* line as a consequence of a pole collapse can be obtained considering the probabilities of failure of each pole at time *t* as follows.

$$P^{P}_{ij,t} = 1 - \prod_{k=0}^{N^{Poles}_{ij}} (1 - P_{k,ij,t}), \forall (ij) \in \Omega_L \, \forall t \in T \tag{1}$$

where $P_{k,ij,t}$ is the probability of failure of the *kth* pole in each *ij* line at each time *t*, and N^{Poles}_{ij} is the number of poles in each *ij* line. As it is considered that either a tower or branch collapse implies the entire line out-of-service, the probability of failure of this *ijth* line is [23,45]:

$$P^{L}_{ij,t} = P^{P}_{ij,t} + P^{B}_{ij,t} - P^{P}_{ij,t} P^{B}_{ij,t}, \forall (ij) \in \Omega_L \forall t \in T \tag{2}$$

wherein $P^{P}_{ij,t}$ and $P^{B}_{ij,t}$ are the probability of failure of the *ijth* line due to pole collapse and wire failure, respectively. Without loss of generality, the span between poles varies according to the types of poles enduring the wires, yet as a rule of thumb, a 100-m span is usually considered the average value in distribution networks. Although the effect that an additional mechanical effort caused by a tower collapse can have on those upstream and downstream cannot be ruled out, this effect has been neglected in this study, assuming the failure probabilities are independent of one another [46]. It is worth noting, though, that this assumption has been made in transmission network studies based on practical experience in the UK [47].

3. Proposed resilience framework

3.1. Overview

This Section details the main characteristics of the three-stage resilience assessment object of study used to lessen the effects of windstorms in distribution networks. The first part describes the flowchart of the proposed framework. Afterwards, the following sections provide the main features of the mathematical formulation considered in the second stage and the voltage regulation of the third, respectively.

3.2. Flowchart of the three-stage resilience assessment

The flowchart of the proposed framework is shown in Fig. 1, where each stage has been encircled with a different colour. Concretely, the first stage is essentially focused on determining the damaged assets at each time instant of the evaluation period by using the curves described in Section 2 and the wind profile retrieved from the meteorological agency [48] (See Fig. 2). As the windstorm unfolds, the set of unavailable lines is determined according to a pre-set vulnerability threshold (i.e., p_{thr}), which has been selected according to the sensitivity analysis provided in Section 4.4.

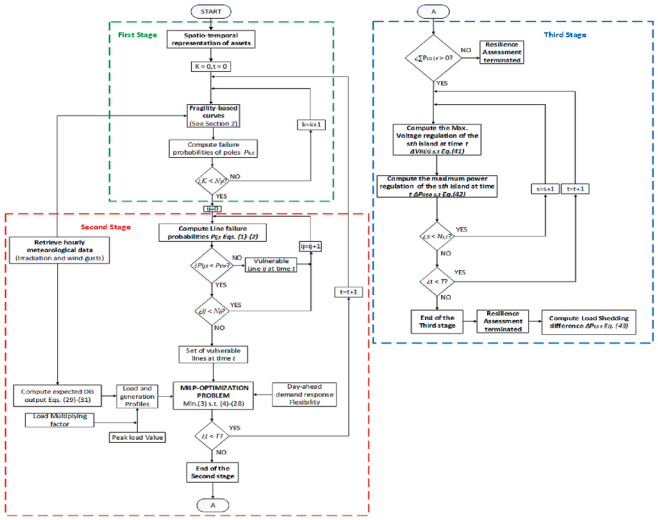

Fig. 1. Flowchart of the proposed three-stage resilience assessment.

Upon completion of the first stage, the lines out-of-service at each time of the assessment are known and therefore used as input for the next stage. After that, given a forecasted non-dispatchable generation profile, the second stage determines the optimal grid configuration including the number of islands, sets the required flexibility and schedules the BESSs. Crucially, the expected load shedding (if any) is obtained in this stage. The objective function, the constraints and main parameters of the deterministic problem are described in Section 3.3.

In case a positive load shedding value has resulted from the second stage, the third stage takes effect to reduce such value by applying a novel voltage regulation scheme wherein the main pillar is the nature of the DGs and BESSs. The specifics of this strategy are extensively discussed in Section 3.4, whereas the feasibility of the proposed scheme is further validated through time-domain simulations for a given test system in Section 4.5. Additionally, the required metrics to measure the benefits offered by the third stage of the approach in terms of load shedding reduction are provided in Section 3.5.

3.3. Stage 2: Mathematical formulation

The deterministic mixed-integer linear programming problem included in the second stage of the proposed approach can be formulated as follows.

$$\min_{V} \sum_{t \in T} \left(\sum_{i \in \Omega_B} (P^{LS}_{i,t} \cdot C^{LS}) + (P^{FL}_{i,t} \cdot C^{FL}) + (P^{SU}_{i,t} \cdot C^{SU}) + (Q^{LS}_{i,t} \cdot C^{LS}) + (Q^{FL}_{i,t} \cdot C^{FL}) + (Q^{SU}_{i,t} \cdot C^{SU}) \right) \tag{3}$$

s.t.

$$P^{ESSC}_{i,t} + P^{L}_{i,t} - P^{DER}_{i,t} - P^{LS}_{i,t} - P^{FS}_{i,t} - P^{ESSD}_{i,t} - P^{SU}_{i,t} = \sum_{j \in \Omega parent,i} P_{j,t} - \sum_{h \in \Omega child,i} P_{hi,t}, \quad \forall i \in \Omega_B, \forall t \in T \tag{4}$$

$$Q^{L}_{i,t} - Q^{DER}_{i,t} - Q^{ESS}_{i,t} - Q^{LS}_{i,t} - Q^{FS}_{i,t} - Q^{SU}_{i,t} = \sum_{j \in \Omega parent,i} Q_{j,t} - \sum_{h \in \Omega child,i} Q_{hi,t}, \quad \forall i \in \Omega_B, \forall t \in T \tag{5}$$

$$(1 - \alpha_{ij,t}) \cdot -M \leqslant V_{i,t} - V_{j,t} - \left(\frac{P_{ij,t} \cdot r_{ij} + Q_{ij,t} \cdot x_{ij}}{V_o} \right) \leqslant (1 - \alpha_{ij,t}) \cdot M, \quad \forall (i,j) \in \Omega_L, \forall t \in T \tag{6}$$

$$0 \leqslant S_{ij,t} \leqslant \alpha_{ij,t} \cdot S^{max}_{ij}, \quad \forall (i,j) \in \Omega_L, \forall t \in T \tag{7}$$

$$S_{ij,t} = \sqrt{P^2_{ij,t} + Q^2_{ij,t}}, \quad \forall ij \in \Omega_L, \forall t \in T \tag{8}$$

$$V^{\min} \leqslant V_{i,t} V^{\max}, \quad \forall i \in \Omega_B, \forall t \in T \tag{9}$$

$$P^{DER\min}_{i,t} \leqslant P^{DER}_{i,t} \leqslant P^{DERmax}_{i,t}, \quad \forall i \in \Omega^{DER}, \forall t \in T \tag{10}$$

$$Q^{DER\min}_{i,t} \leqslant Q^{DER}_{i,t} \leqslant Q^{DERmax}_{i,t}, \quad \forall i \in \Omega^{DER}, \forall t \in T \tag{11}$$

$$S^{DER}_{i,t} = \sqrt{\left(P^{DER}_{i,t}\right)^2 + \left(Q^{DER}_{i,t}\right)^2}, \quad \forall i \in \Omega^{DER}, \forall t \in T \tag{12}$$

$$0 \leqslant P^{FL}_{i,t} \leqslant P^{FLmax}_{i,t}, \quad \forall i \in \Omega_B, \forall t \in T \tag{13}$$

$$0 \leqslant Q^{FL}_{i,t} \leqslant Q^{FLmax}_{i,t}, \quad \forall i \in \Omega_B, \forall t \in T \tag{14}$$

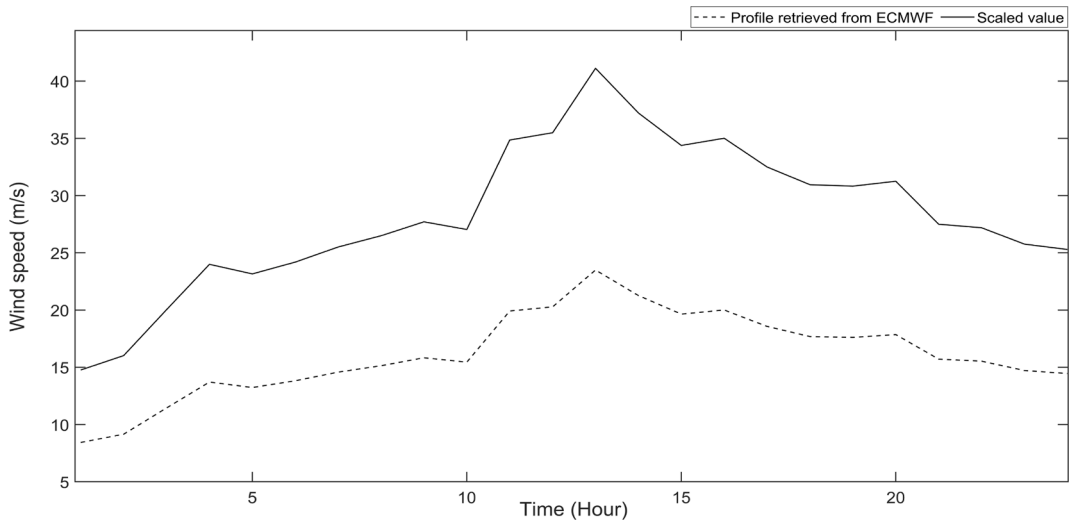

Fig. 2. Wind Profiles; Retrieved and scaled.

$$0 \leqslant P_{i,t}^{LS} \leqslant P_{i,t}^{L}, \quad \forall i \in \Omega_B, \forall t \in T \tag{15}$$

$$0 \leqslant Q_{i,t}^{LS} \leqslant Q_{i,t}^{L}, \quad \forall i \in \Omega_B, \forall t \in T \tag{16}$$

$$0 \leqslant P_{i,t}^{LS} + P_{i,t}^{FL} \leqslant P_{i,t}^{L}, \quad \forall i \in \Omega_B, \forall t \in T \tag{17}$$

$$0 \leqslant Q_{i,t}^{LS} + Q_{i,t}^{FL} \leqslant Q_{i,t}^{L}, \quad \forall i \in \Omega_B, \forall t \in T \tag{18}$$

$$0 \leqslant P_{i,t}^{SU} \leqslant P_{i,t}^{SUmax}, \quad \forall i \in \Omega_B, \forall t \in T \tag{19}$$

$$0 \leqslant Q_{i,t}^{SU} \leqslant Q_{i,t}^{SUmax}, \quad \forall i \in \Omega_B, \forall t \in T \tag{20}$$

$$SOC_{i,t} = SOC_{i,t-1} + \eta_{i,t}^{c} \cdot P_{i,t}^{ESSC} - \frac{P_{i,t}^{ESSD}}{\eta_{i,t}^{d}}, \quad \forall i \in \Omega^{ESS}, \forall t \in T \tag{21}$$

$$SOC_{i,t}^{\min} \leqslant SOC_{i,t} \leqslant SOC_{i,t}^{\max}, \quad \forall i \in \Omega^{ESS}, \forall t \in T \tag{22}$$

$$P_{i,t}^{ESSC\min} \delta_{i,t}^{C} \leqslant P_{i,t}^{ESSC} \leqslant P_{i,t}^{ESSC\max} \delta_{i,t}^{C}, \quad \forall i \in \Omega^{ESS}, \forall t \in T \tag{23}$$

$$P_{i,t}^{ESSD\min} \delta_{i,t}^{D} \leqslant P_{i,t}^{ESSD} \leqslant P_{i,t}^{ESSDmax} \delta_{i,t}^{D}, \quad \forall i \in \Omega^{ESS}, \forall t \in T \tag{24}$$

$$\delta_{i,t}^{C} + \delta_{i,t}^{D} \leqslant 1, \quad \forall i \in \Omega^{ESS}, \forall t \in T \tag{25}$$

$$S_{i,t}^{ESS} = \sqrt{\left(P_{i,t}^{ESSC} + P_{i,t}^{ESSD}\right)^2 + Q_{i,t}^{ESS,2}}, \quad \forall i \in \Omega^{ESS}, \forall t \in T \tag{26}$$

$$P_{i,t}^{L} = P_{i,t}^{o}\left(\frac{V_{i,t}^2}{V_i^o} Ki, Z + \frac{V_{i,t}}{V_i^o} Ki, I + Ki, P\right), \quad \forall i \in \Omega_B, \forall t \in T \tag{27}$$

$$Q_{i,t}^{L} = Q_{i,t}^{o}\left(\frac{V_{i,t}^2}{V_i^o} K'i, Z + \frac{V_{i,t}}{V_i^o} K'i, I + K'i, P\right), \quad \forall i \in \Omega_B, \forall t \in T \tag{28}$$

$$P_{i,t}^{W} = \begin{cases} 0 & u_t < u_{cut-in} \\ P_i(u_t) & u_{cut-in} \geq u_t > u_{rated} \\ P_i^{rated} & u_{rated} \geq u_t > u_{cut-off} \\ 0 & u_t \geq u_{cut-off} \end{cases} \forall i \in \Omega^{DER}, \forall t \in T \tag{29}$$

$$T_t^c = T^{amb} + \left(T^{sd}/800\right) * I_t^r \quad \forall i \in \Omega^{DER}, \forall t \in T \tag{30}$$

$$P_{i,t}^{PV} = P_i^{peak} * \left(I_t^r / I^{sd}\right) - apv * \left(T_t^c - T^{sd}\right) \forall i \in \Omega^{DER}, \forall t \in T \tag{31}$$

The objective function in (3) minimises the cost of the distribution network restoration, where the costs are the energy supplied by the main grid, the load shedding and the flexibility as part of a demand response program. The non-dispatchable DERs (i.e., PV and wind) and BESSs have been assumed to be zero. The decision variables of the raised optimization problem are denoted by V in (3) and are as follows; $\{P_{i,t}^{DER}, Q_{i,t}^{DER}, S_{i,t}^{DER}, P_{ij,t}, Q_{ij,t}, S_{ij,t}, P_{i,t}^{L}, Q_{i,t}^{L}, P_{i,t}^{FL}, Q_{i,t}^{FL}, P_{i,t}^{LS}, Q_{i,t}^{LS}, P_{i,t}^{ESSD}, P_{i,t}^{ESSC}, Q_{i,t}^{ESS}, SoC_i, {}_t, P_{i,t}^{SU}, Q_{i,t}^{SU}, V_{i,t}, \delta_{i,t}^{C}, \delta_{i,t}^{D}\}$.

Equations (4) and (5) represent the nodal balance constraints for both active and reactive power, respectively. In this equation $P_{i,t}^{L}$ and $Q_{i,t}^{L}$ are the rated active and reactive power load considering the voltage-dependency load model, whilst $P_{i,t}^{o}$ and $P_{i,t}^{o}$ correspond to the load values at the rated voltage, respectively. The terms $P_{i,t}^{SU}$ and $Q_{i,t}^{SU}$ stand for the energy provided by the upstream grid, being zero in all buses except for the main substation. The power flow is expressed in (6). As can be seen, a linearised version of the AC power flow has been regarded, where the voltage angle is neglected. More details of the DistFlow model applied in distribution networks can be found in [49]. The maximum current flowing through the distribution lines is dictated by the cross-section and introduced as a constraint in (7) and (8). It is worth noting that the binary variable α is an input parameter in this process, as has been derived in the first stage. Constraint (9) limits the voltage magnitudes between $V^{\max}$ and $V^{\min}$. Constraints (10) and (11) stand for the maximum and minimum outputs of the non-dispatchable DERs, where the apparent power cannot exceed (12). It has been considered that these units cannot be operated above the active power available in each time instant yet can be curtailed. The reactive power delivered by capacitor banks placed along the grid is included in the term $Q_{i,t}^{DER}$. On the other hand, the maximum apparent power delivered by DERs is dictated by (12). Constraints (13) and (14) take into consideration the maximum available flexibility for both active and reactive powers at each bus. The maximum load to be shed in each bus cannot exceed the load value of that bus according to (15) and (16). Furthermore, since the load to be curtailed cannot be above the sum of both flexibility and load shedding terms, constraints (17) and (18) have also been considered. The amount of energy exchanged with the main grid has also been limited to both upper and lower limits in (19) and (20), respectively. The state of charge of each BESS unit is computed as (21) and constrained by (22). The maximum instantaneous power delivered for either charging or discharging is controlled in (23) and (24).

In order to avoid simultaneous charging and discharging, two binary variables must be included in (25). The apparent power delivered by the BESSs through the voltage source converter is limited in (26). The voltage-dependency load model is given by (27–28).

The power delivered by the non-dispatchable wind turbines is

calculated through the piece-wise linear function in (29) [50], whereas the PV units are modelled as in (30) and (31) [51].

The optimisation problem in (3)-(27) is also complemented with logical constraints to determine whether to assign the root of the island to either DER or BESSs. Hence, if the grid is affected by an "*N-k*", we will have *k* isolated portions being potential islands where only one root is allowed on each one. As can be seen in the snippet of Table 2, the voltage of the root in each island is assigned to 1 p.u. at each time *t* and belongs to the unit (either DER or BESS) with larger output. The substation has been considered unloaded, and islands where any source is available (including those where the SOC of the BESS is zero), are assumed to be de-energised, and consequently, all buses will experience load shedding and voltage is assigned to $V^{\min}$.

3.3.1. Linearisation procedure

Since some parameters in Eqs. (8), (12) and (26) have non-linear terms, a linearisation process is required if these constraints are to be considered in the mixed integer linear program (MILP) of the second stage. In this paper, both the BESSs and non-dispatchable DERs are expected to engage in voltage regulation and deliver both active and reactive power, as seen in (32)-(35). Similarly, if the power flow along the distribution branches is to be considered as a constraint, it must also undergo a linearisation process. To that purpose, as this value is largely active [30], the following arrangement in (36) and (37) has been introduced. Based on the previous assumptions, the summary of the linearised equations is listed below.

$$P_{i,t}^{DER\max} = S_{i,t}^{DER\max}, \quad \forall i \in \Omega^{DER}, \forall t \in T \tag{32}$$

$$Q_{i,t}^{DER\max} = S_{i,t}^{DER\max} \cdot 0.1, \quad \forall i \in \Omega^{DER}, \forall t \in T \tag{33}$$

$$P_{i,t}^{ESS\max} = S_{i,t}^{ESS\max}, \quad \forall i \in \Omega^{ESS}, \forall t \in T \tag{34}$$

$$Q_{i,t}^{ESS\max} = S_{i,t}^{ESS\max} \cdot 0.1, \quad \forall i \in \Omega^{ESS}, \forall t \in T \tag{35}$$

$$P_{ij,t}^{\max} = S_{ij,t}^{\max} \cdot 0.95, \quad \forall ij \in \Omega_L, \forall t \in T \tag{36}$$

$$Q_{ij,t}^{\max} = S_{ij,t}^{\max} \cdot 0.5, \quad \forall ij \in \Omega_L, \forall t \in T \tag{37}$$

Additionally, the voltage-dependency load modelling in (27)-(28) includes a non-linear term, yet considering the common range of voltages in distribution networks (i.e., in the range of 0.9 p.u. and 1.05 p.u.), the subsequent linearisation can be implemented, see [28];

$$P_{i,t}^{L} = P_{i,t}^{o}\left(2\left(V_i^o - V_{i,t}\right)Ki, Z + \frac{V_{i,t}}{V_i^o}Ki, I + Ki, P\right), \quad \forall i \in \Omega_B, \forall t \in T \tag{38}$$

$$Q_{i,t}^{L} = Q_{i,t}^{o}\left(2\left(V_i^o - V_{i,t}\right)K'i, Z + \frac{V_{i,t}}{V_i^o}K'i, I + K'i, P\right), \quad \forall i \in \Omega_B, \forall t \in T \tag{39}$$

3.4. Stage 3: Voltage regulation scheme

The main goal of this Section is to reduce the load shedding obtained in the first stage, if any, by adding a certain active-power imbalance in each island energised by a DER, BESSs or a combination of both. As has been reported in [52,53], an active-power mismatch between generation and load in an island that is composed of electronically interfaced devices results in a voltage deviation according to the following relationship:

$$\Delta V = \sqrt{\Delta P \cdot PDER} \tag{40}$$

where ΔV is the voltage drop in an island, ΔP is the active power imbalance between generation and load, and P_{DER} is the instantaneous power delivered by the converter-based DER (note that BESS also falls within this casuistry). As illustrated in the flowchart of Fig. 1, the outcomes of the second stage provide the data of each island, including the buses, the roots and the available DERs and BESSs.

The maximum voltage to be used in the power regulation scheme in each *sth* island at every time slot *t* is as follows:

$$\Delta V_{s,t}^{REG} = \Delta V_{MAX} - \Delta V_{s,t}, \forall s, t \in \Omega_{s,t} \tag{41}$$

where $\Delta V_{s,t}^{REG}$ is the maximum voltage regulation in each island, ΔV_{MAX} is the maximum voltage drop allowed in the distribution network (e.g., 0.1 p.u. in this case) and $\Delta V_{s,t}$ represents the maximum voltage drop along the distribution lines on each *sth* island.

The maximum active power to be utilised by the voltage regulation scheme in each island can be rewritten using Eq. (40) and considering that each island has been assigned a root:

$$\Delta P_{s,t}^{REG\max} = 1 - (V\min + \Delta V_{s,t})^2, \forall s, t \in \Omega_{s,t} \tag{42}$$

where $\Delta P_{s,t}^{REG\max}$ and $\Delta V_{s,t}$ represent the maximum power that can be used by this scheme and the maximum voltage drop in each *sth* island at time *t*, respectively.

3.5. Metrics to evaluate the voltage regulation scheme

As this article proposes a voltage reduction to lessen the load shedding obtained in the aftermath of the windstorm, the difference between the second and third stages defines the improvement in resilience. Thence, the effectiveness of the suggested approach can be expressed by the equation defined below:

$$\Delta P_t^{LS} = \left(1 - \frac{\sum_{i=1}^{NB} P_{i,t}^{LS} - \sum_{s=1}^{N_t^{Islands}} \Delta P_{s,t}^{REG}}{\sum_{i=1}^{NB} P_{s,t}^{LS}}\right) x100\,, \forall t \tag{43}$$

where ΔP_t^{LS} stands for the reduction in load shedding between stages, $\Delta P_{s,t}^{REG}$ the active power used by the voltage scheme and $P_{s,t}^{LS}$ ensues from the outcomes of the optimization problem in the second stage.

Table 2
Pseudocode to determine the feasible islands at each time step.

Steps Determining the roots on each island
Inputs;$\Omega_L, \alpha_{ij,t}, P_{i,t}^{ESSD}, P_{i,t}^{ESSC}, P_{i,t}^{W}, P_{i,t}^{PV}$ **Outputs;**$\Omega_{s,t}, \Omega_{s,t}^{root}$
1. Update values
2. For $i = 1$: T
3. find$\alpha_{ij,t} = 0$ and determine both $N_t^{Islands}$ and $\Omega_{s,t}$
4. end
5. For s = 1:$N_t^{Islands}$
6. find max $\{P_{i,t}^{ESSD}, P_{i,t}^{ESSC}, P_{i,t}^{NDG}\}$ and determine $\Omega_{s,t}^{root}$
7. Assign V ($\Omega_{s,t}^{root}$) = 1 p.u.;
8. end

4. Numerical simulations

4.1. Test system and components modelling

In this Section, the algorithm described in Section 3 is perused with numerous scenarios in a modified version of the IEEE 33-bus test system where DGs and BESSs have been added, having all tie switches open. A set of wind-based non-dispatchable DERs have been added on buses 18, 25 and 31 with a rated power of 0.1 MW,0.2 MW and 0.9 MW, respectively. The cut-off speed for the wind turbines is set at 24 m/s. The line impedances and peak load data have been retrieved from [30].

On the other hand, PV-based DERs are allocated at buses 11 and 20 with a rated power of 0.6 MW and 0.9 MW, respectively. The BESSs total power is 2.6 MW, although how this amount is distributed across the system depends on the considered scenario, as is seen in subsections 4.2.1 and 4.2.2, respectively. The capacity of each BESS unit has.

been set to 10 times the instantaneous power (i.e., 0.1 MW unit is 1 MWh). A random multiplying factor in the range of max/min 1.1/0.45 has been used to establish the daily load profile considering the peak

value of 3.715/2.3 MW/MVAr as a base case. The demand-side response represents 13 % with respect to the peak load value, and it is only available on buses 14, 20, 28 and 30. It is worth noting that this maximum flexibility value has been kept constant throughout the assessment. The maximum and minimum voltage magnitudes allowed in this paper are set out to 1.05/0.9 p.u., respectively. The cross-section of each branch dictates the implemented limitation in the power flow. The constants in (38)-(39) account for the share of each load model (i.e., constant impedance, constant current and constant power) for both active and reactive power being 0.24, 0.62, 0.13, and 2.44, −1.94, 0.5, respectively. The time-series wind data used in this article belong to the meteorological conditions that occurred on the 27th of February 2022 over the storm EUNICE at the isle of Wight, where the highest wind gust was recorded [54]. As indicated in [23], the available 10-m wind profiles may not match the recorded 3 s wind gusts as it is hourly averaged. To such a purpose, it seems reasonable to scale up such a profile to represent a realistic scenario, see Fig. 2. A total period of 24 h has been simulated, where the wind picks up as the event unfolds, as illustrated in Fig. 2. All scenarios used for the optimisation simulations were executed on a PC with Intel 9-core CPU 3.6 G Hz. The proposed MILP model was solved using IBM ILOG CPLEX 12.4 run in the Matlab environment, including a 10^{-5} relative optimality gap.

The maximum computational time proved to be 3.2 s when solving case 4. Please note that the rest of the parameters are those established by default by the solver.

4.1.1. Additional assumptions deemed in the optimization model

Besides the information provided in the previous Section, the following assumptions were taken into consideration to solve the optimisation problem:

- It is considered that the DERs are equipped with grid-forming capabilities and, therefore, able to run an island after the grid configuration has been determined.
- The PV and wind DERs always operate at the maximal power point (MPP) in both normal and outage conditions. The forecast error of hourly-average solar irradiance and wind profiles is neglected. The DERs and BESSs operating cost has been assigned to zero. Since the obtained profiles do not significantly differ between different longitudes and latitudes within the island, the same wind speed and solar irradiance profiles are used.
- The distribution poles have been considered 10 m in height, avoiding the need to scale up the wind values retrieved from [54]. Even though the angle can be computed by means of the two wind components (i.e., eastwards/westwards and northwards/southwards), a 90 degrees angle has been selected in this paper as it is regarded to be the most unfavourable scenario.
- It has been contemplated that a line cannot be repaired given the time frame of 24 h considered in this paper, so all those lines are considered down from the moment they are above the established p_{th} in each case.
- If any source is energising an isolated portion of the grid, that is, whether because the SOC of the BESS is zero or there are no DERs, such a portion does not constitute an island.
- The reactive power curtailment has not been scouted as it is linked with frequency [52], which is considered fixed in this assessment. This is demonstrated in Fig. 12 of Section 4.5, where the frequency is controlled by the grid-forming devices.

4.2. Considered scenarios

The three-stage resilience assessment has been tested with the wind profile displayed in Fig. 2, which results in the line failure probabilities shown in Fig. 10. Given these failure probabilities, if we consider two main scenarios with two different vulnerability thresholds, we have a total of 4 case studies. The main features of each scenario and its outcomes are summarised and detailed in Subsections 4.2.1 and 4.2.2. It is worthwhile to note that the main difference between scenarios lies in how the BESSs units are located along the distribution system, keeping the total amount constant. Note that the non-dispatchable units (either PV or wind-based) and load data detailed in the previous Section 4.1 are also the same for all scenarios.

4.2.1. Scenario 1

In this scenario, the BESS units have been allocated in buses 11, 18, 19, 22, 25 and 31, corresponding to a rated active power of 0.2 MW, 0.4 MW, 0.3 MW, 0.1 MW, 1 MW and 0.6 MW. Within the same scenario, two vulnerability thresholds have been regarded, resulting in cases 1 and 2 (i.e., p_{th} equals 0.1 p.u. and 0.05 p.u., respectively). The first case implies that line 17 is out of service at t = 11 and lines 2, 8, 12, 13, 15,16,17,18, 20 and 27 at t = 13. Given the number of lines tripped in the first case, bus 18 operates as an island from t = 11 on, finally equating to six islands at t = 13. For the sake of clarity, the set of six islands in case 1 comprises the following buses: island 1 (buses 3 through 8 and 23 through 27), island 2 (buses 9 through 12), island 3 (bus 18), island 4 (buses 19 and 20), island 5 (buses 21 and 22) and island 6 (buses 28 through 33). Additionally, Fig. 3 illustrates the grid partitioning obtained in this case, including the abovementioned six islands.

The voltage profile obtained in the first case is displayed in Fig. 4 (a), where the formation of an island at bus 18 is identified at t = 11, whereas from t = 13 on, six islands are obtained. The load shedding obtained on each island is depicted in Fig. 5 (a) for both the second and third stages. As can be seen, by using the voltage scheme included in the third stage, the load shedding has been slightly reduced in islands 1 and 5 and completely removed in islands 2 and 6. Note, however, that the values in islands 3 and 4 are not displayed as the load shedding in the second stage is zero, and the assessment is therefore terminated at that stage (See the Flowchart in Fig. 1). To provide a clear understanding of how the power has been restored on each island, the power regulation is displayed separately in Fig. 5 (b). It is interesting to highlight the fact that according to Eq. (42), the power regulation varies according to the maximum voltage that this scheme can commit based on the voltage drop in each island throughout the 24-h period. In this vein, islands with a large number of buses could experience larger voltage drops, thus reducing the voltage margin available in this scheme (e.g., see values for island 1 in Fig. 5 (b)).

Secondly, as can be expected, the lower the vulnerability threshold, the larger the number of lines considered damaged. Concretely, in case 2, line 17 is out of service at t = 9, followed by lines 12, 17, 20 and 27 at t = 11 and finally, the rest of the lines except those underground (i.e., 30, 31 and 32) are also tripped at t = 13. In the aftermath of the second case study, bus 18 is islanded between t = 9 and t = 13, 5 islands are obtained between t = 11 and t = 13, and 29 islands are eventually operated from t = 13 onwards.

The voltage profile obtained in the second case is displayed in Fig. 4 (b), where the formation of an island on bus 18 is identified at t = 11, and six islands are obtained from t = 13, which correspond to the buses with either DERs or BESSs given the fact that 29 lines are tripped in this case. In this case, feasible islands occur only in buses with embedded generation, leading to a large amount of generation that needs to be curtailed to fulfil the nodal balance, thus implying zero load shedding in those buses yet large values in the rest of de-energised buses. This explanation is in accord with the results depicted in Fig. 5, where the difference in load shedding between stages is very narrow as the second stage barely takes part.

For the purpose of comparing and evaluating, the outcomes of the load shedding in both cases, 1 and 2, are exhibited in Fig. 6, wherein solid lines represent those obtained in the second stage and dashed ones belong to those obtained after applying the third stage.

4.2.2. Scenario 2

In this Scenario, the total amount of power assigned to the BESSs in

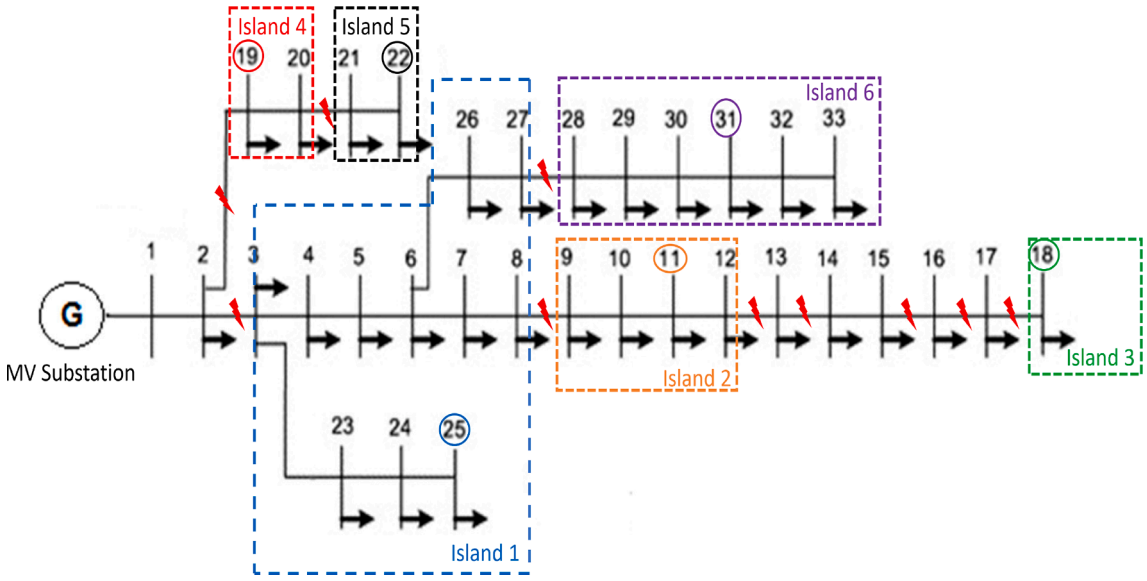

Fig. 3. Representation of the 6 islands originated in Scenario 1-Case 1.

the previous scenario has now been scattered along the 33 buses, having 32 small units of 0.087 MW in each bus. In addition to that, two vulnerability thresholds are used to obtain cases 3 and 4 (i.e., p_{th} 0.1 p.u. and 0.05 p.u., respectively). Given that only one wind profile is used in this paper, the damaged lines in the current scenario are the same as those analysed in the previous scenario, yet with a different number of islands and configurations. That is to say, cases 3 and 4 have the same lines out of service as in cases 1 and 2, respectively. Hence, in addition to the six islands given in case 1 of the first scenario, four more have now been introduced; island 7 belongs to bus 13, island 8 entails buses 14 and 15, whereas islands 9 and 10 belong to buses 16 and 17, respectively.

Crucially, though, in case 1, the power could not be restored in buses 13 through 17 as lines 12, 13, 15, 16 and 17 were tripped, and no generation was in place. In this case, the load in those buses can be picked up as part of the intentional islanding operation. Such insight can be observed in the voltage profile in Fig. 7 (a). Those islands with load shedding larger than zero after the second stage are illustrated in Fig. 8 (a). As observed, using the voltage scheme included in the third stage, the load shedding has been narrowly reduced in island 5 yet significantly ameliorated in islands 1 and 6. Please, that the results for the rest of the islands are not displayed as the load shedding is zero after the second stage.

The voltage results in case 4 are shown in Fig. 7 (b), where voltages are around 1 p.u., as 29 islands are obtained at t = 13. In a bid to unnecessarily extend the manuscript and given the number of islands, in this case, only the total load shedding is provided where, at the same time, is compared with case 3, see Fig. 9.

4.3. Results discussion

In general, from the results provided in the previous Sections 4.2.1 and 4.2.2, it can be drawn that the load shedding has notably been reduced with the three-stage proposed approach without violating the voltage constraint (9) in the MILP program. Specifically, the BESS units have been allocated in few buses in Scenario 1 and unanimously distributed in Scenario 2, thus giving different "*N-k*" values if two vulnerability thresholds are considered (i.e., cases 1 through 4). The results of these cases are summarised in Table 4. The values in the fifth column provide the load shedding obtained in the second stage of the proposed methodology for both active and reactive power, whilst the fifth and sixth illustrate the percentage of improvement when the proposed approach is applied.

It is worth highlighting that, even though case 1 obtains a significant reduction in load shedding, the proposed scheme is particularly effective when the grid is split into multiple islands along the grid with dispersed BESSs, see cases 3 and 4. In fact, if one compares the voltage profiles between scenarios 1 and 2 after t = 10, one will notice the benefits of scattering the BESSs in multiple microgrids. On the other hand, as seen in case 2, when the windstorm causes large "*N-k*" values and both DERs and BESSs are allocated in just a few buses, no major improvement is observed.

4.4. Threshold selection for vulnerability; a sensitivity analysis

This article takes advantage of the so-called fragility curves to determine the "*N-k*" at each time step, wherein the wind speed is the main control variable. The status of each line is determined by an offline vulnerability threshold, as mentioned in the previous Section given the wind profile. Crucially, setting this threshold is a trade-off between the risk of overreacting when it is chosen very low and the risk of misidentifying the effects of such an eventuality if it is high. Although it is normally the operator who takes responsibility for this managerial decision, in this paper, a sensitivity analysis has been conducted to evaluate the influence of this value on the outcomes of the resilience assessment.

As is illustrated in Fig. 10, as the wind picks up during the event, the probabilities of failure increase accordingly, yet significant differences are observed depending on the configuration of each line (i.e., types of poles and their ages). Specifically, lines 17, 18, 25 and 27 can be categorised as highly vulnerable, reaching 0.32 p.u.,0.55 p.u., 0.44 p.u. and 0.43 p.u. at the peak of the event (i.e., t = 13), respectively. These lines are more vulnerable as they include both aged class 3 wood poles and leaned poles. On the contrary, for example, lines 4, 5, and 6 are mainly composed of new steel poles and are inherently more robust. Given both the wind profile and the spatiotemporal representation defined in Section 2 as main inputs, four thresholds are considered, as seen in Fig. 11. The charts displayed in Fig. 11 give evidence that there are no noticeable differences between 0.2 p.u. and 0.15 p.u. It is noteworthy to say that all lines are above 0.05 p.u., as only underground lines can withstand the event when it is at its maximum value. Therefore, in order to consider a realistic approach, it seems reasonable to select both 0.05 p.u. and 0.1 p.u. given the fact that all failure probabilities fall within this range. The number of lines tripped in Fig. 11 just represents the instant of time when a line has surpassed a particular threshold. Yet however, as

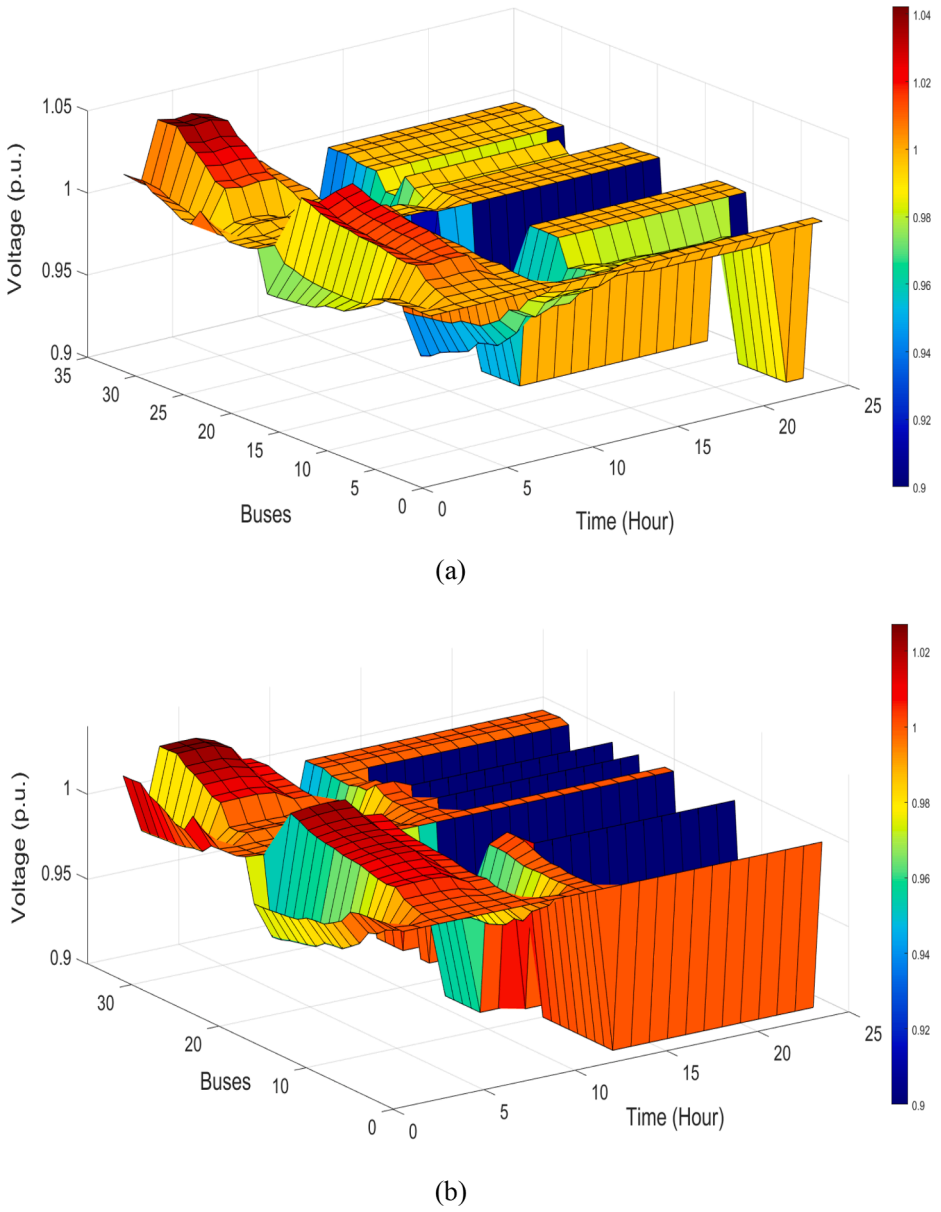

Fig. 4. Voltages obtained in Scenario 1. (a) Case 1, (b) Case 2.

mentioned in Section 4.2, a line is considered damaged from the instant it exceeds the established threshold.

4.5. Time-domain simulations

The central goal of this Section is to provide evidence that an additional active-power imbalance is traduced into a voltage imbalance in an island composed of VSC-based DERs, which would prove that the reduction in load shedding proposed in this article can safely be made. Although the feasibility of Eqs. (40) - (43) has already been proven right in [52,53], the current Section provides proof-of-concept of such equations through time-domain simulations. To avoid unnecessarily extending the manuscript, only the first case detailed in Section 4.2.1 has been used for validation purposes. As seen in Section 4.4, the third stage only goes further if load shedding is larger than zero in the second stage, meaning that hours 1 to 10 can be dismissed for the time-domain simulations as all lines are connected. Bearing in mind that such a complex test system in a discrete mode may take excessive computation times, and only the concept is to be validated, it has been decided to consider only a few time instants extracted from the offline assessment. Considering the previous reasoning, a 5 s time-domain simulation has been launched where each hour of the offline assessment represents 1 s. Thence, t = 1 s represents the instant where line 17 is tripped (i.e., t = 11 in the offline assessment), leading to an island at bus 18. Subsequently, at t = 3 s, lines 2, 8, 12, 13, 15,16,17,18 and 27 are tripped, causing the formation of 6 islands, as stated in Section 4.2.1.

It is worth stressing that the BESSs operate as grid-following VSCs before t = 1 s and are switched to grid-forming when the island is intentionally performed. See a detailed analysis of these two operation modes implemented to control VSCs in [55]. The bus voltage magnitudes and frequency of islands 1 through 3 are displayed in each column of Fig. 12. (a), whereas the results of islands 4 through 6 are plotted in each column of Fig. 12 (b), respectively. The first row of Fig. 12 shows the frequency of the islands, and the second the voltage magnitudes of the buses on each island. The third row of pictures zooms into the second row to accurately observe the voltage drops in each island. The results in Fig. 12 are in accord with those in Section 4, where the first island to occur is at bus 18, which belongs to t = 1 s in the simulations. The rest of the islands are formed at t = 3 s (i.e., t = 13 in the offline assessment). From the results, it is seen that islands 1 and 4 are those where the

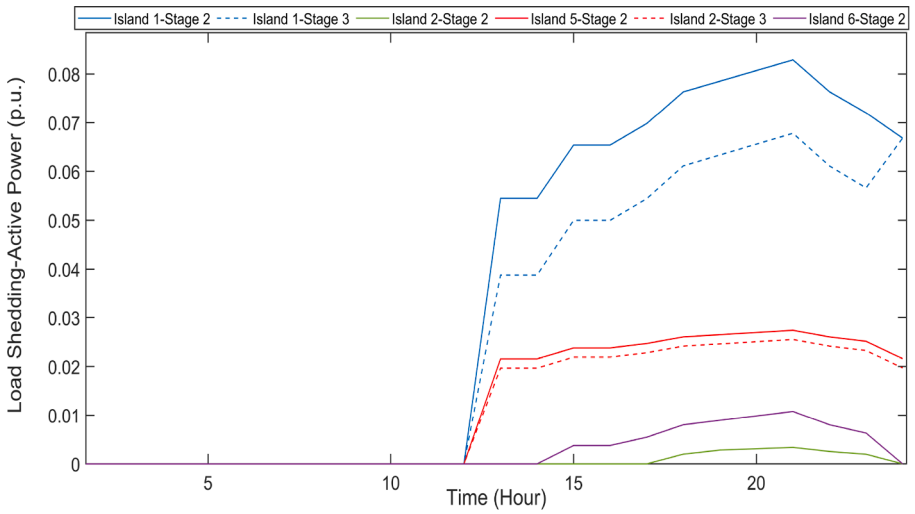

(a)

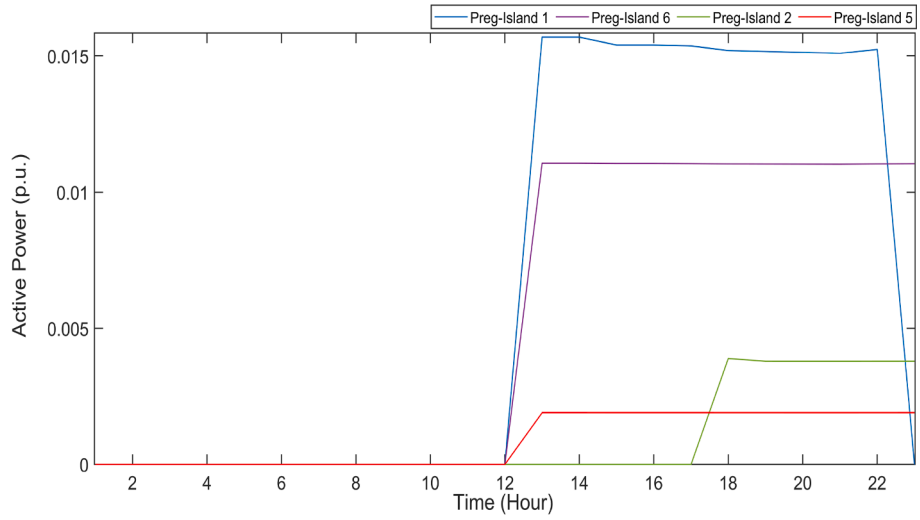

(b)

Fig. 5. Results of Scenario 1-Case 1. (a) Load Shedding, (b) Power regulation.

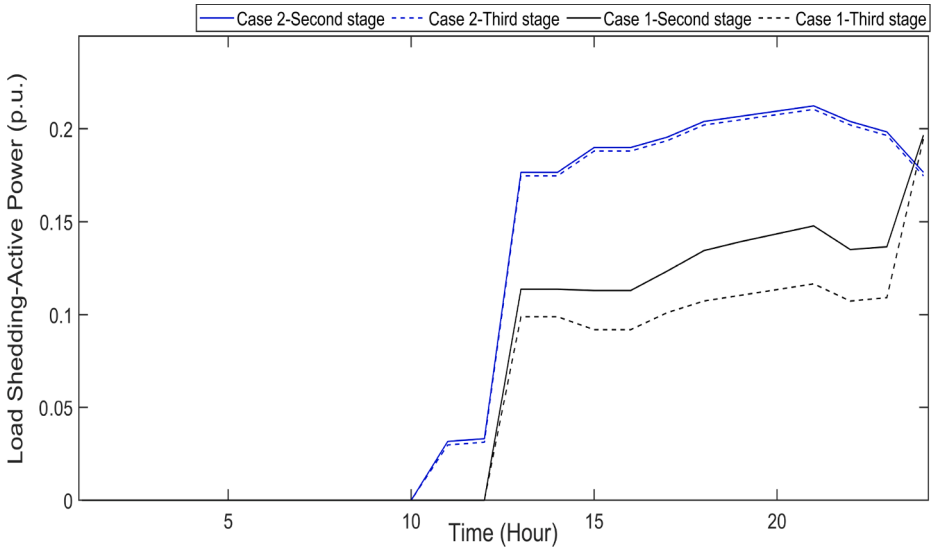

Fig. 6. Load Shedding in cases 1 and 2 of Scenario 1.

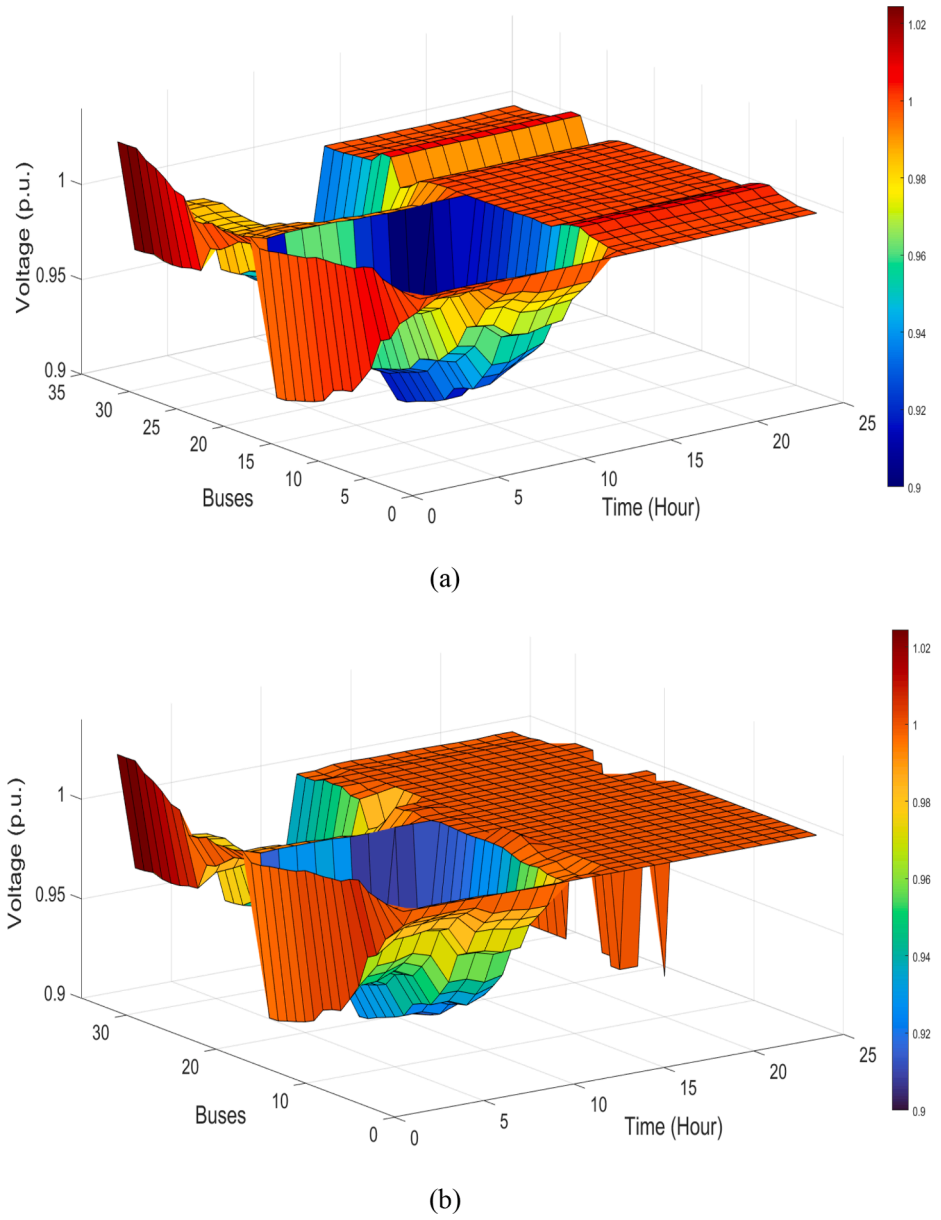

Fig. 7. Voltages obtained in Scenario 2. (a) Case 3, (b) Case 4.

voltage scheme has been applied, as the voltage intentionally drops to near V^{min} after islanding formation.

It is worth noting that before t = 1 s for island 1 and t = 3 s in the rest of the islands, the system remains connected to the grid, and both the BESSs and DERs are operating in a grid-following mode where the main grid dictates the voltage and frequency.

In the time-domain simulations, a three-phase two-level VSC has been implemented and modelled as a switching function controlled by the firing pulses of a PWM generator. The details of the BESSs and PV considered in the time-domain simulations are summarised in Table 5. The time-domain simulations have been conducted within the MATLAB/Simulink environment taking advantage of the power systems toolbox library in a discrete mode with a fixed sample time of 50·μs.

5. Comparison with other existing resilience-oriented approaches

To underscore the benefits of the proposed approach, this Section compares the proposed methodology with some recently published resilience-oriented assessments. In particular, Refs. [28] and [29] are analyzed in the same Section as both addressed windstorms in DNs, whereas [34] and [49] are scrutinized in separate sections.

5.1. Comparison with Refs. [28] and [29]

This Section compares the proposed approach with those included in Refs. [28–29] and highlights the benefits of both the spatiotemporal representation and the proposed three-stage approach deemed in this article. Firstly, the influence of the fragility modelling is scrutinised by comparing the number of lines tripped when the approach in [28] is considered with the spatiotemporal representation accounted for in the present study. Thence, the probabilities of failure are plotted in Fig. 13, where the control variable is the wind profile plotted in Fig. 2. If such a model is used, one can notice that all lines are equally exposed to the windstorm at each hour of the assessment if only one wind profile has been considered, which leads to an unrealistic scenario. As can be seen, when several types of poles and deterioration (e.g., pole ageing and leaning) are modelled, the system becomes more vulnerable.

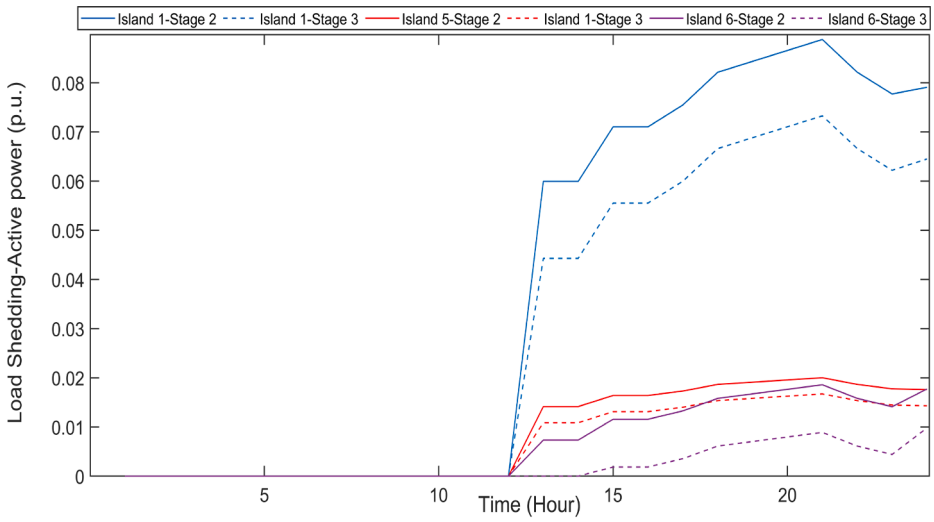

(a)

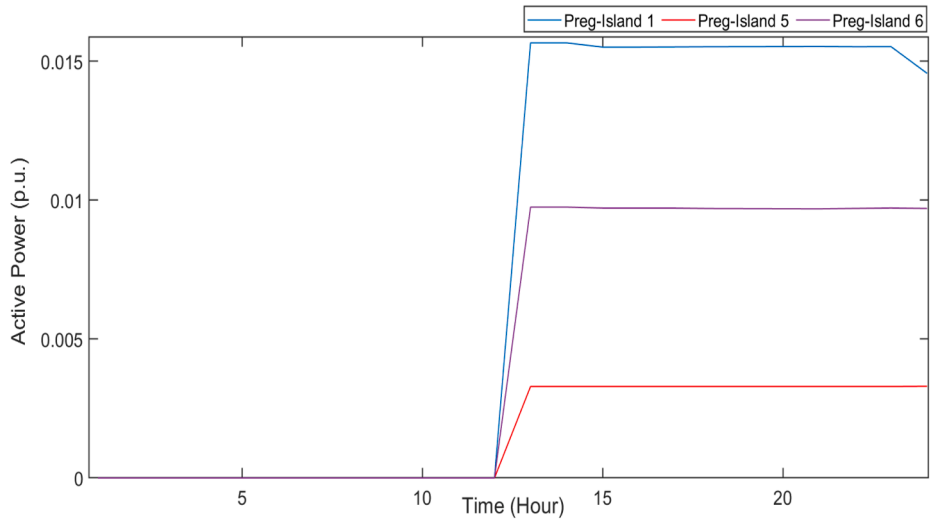

(b)

Fig. 8. Results of Scenario 2-Case 3. (a) Load Shedding, (b) Power regulation.

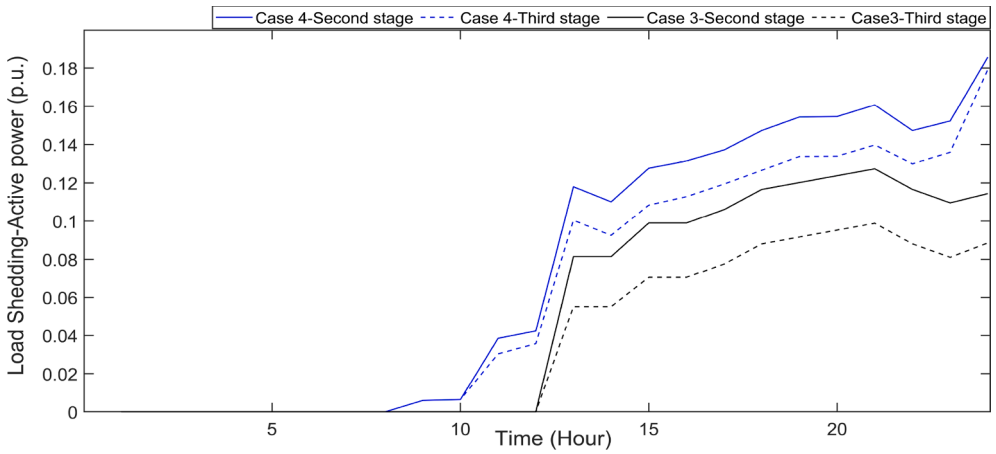

Fig. 9. Load Shedding of cases 3 and 4 in Scenario 2.

Table 4
Summary of the results in Cases 1, 2, 3, and 4 of Section 4.

Case	$p_{th}(p.u.)$	$N\text{-}k$	N^{o} islands	$P_{s,t}^{LS1}/Q_{s,t}^{LS1}(p.u.)$	$\Delta P_{i,t}^{LS}(Percent)$	$\Delta P_{i,t}^{LS}(£)^{*}$
Case 1	0.1	10	6	1.61/0.645	16.6	2680
Case 2	0.05	29	6	2.4/1.25	1.4	265
Case 3	0.1	10	10	1.295/0.58	12.56	2286
Case 4	0.05	29	29	1.81/1.45	25.85	3351

* Price considered for the Load Shedding; 1000 £/MWh.

Furthermore, as demonstrated in the case studies covered in Section 4, the location of the generation resources (i.e., DERs and BESSs) and the faulty lines can play a pivotal role when it comes to grid restoration, as the same number of damaged lines yet different location can certainly give a different picture.

Secondly, the system model used in this paper to test the effectiveness of the proposed approach has been simulated again, yet bringing in the features implemented in [28,29]. To that end, the size and capacity of RESs, BESSs, and load profiles of Section 4.2 have been reutilised for these simulations, and the number of tripped lines has been obtained from each paper, respectively. Accordingly, ten overhead distribution branches resulted damaged as a 5 % vulnerability threshold was deemed in [28] (i.e., lines 2–3,5–6, 6–26, 7–8, 10–11, 14–15, 21–22, 24–25, 30–31, and 31–32), thus leading to 10 islands. The results of the 13th time slot are extracted from the 24-h assessment and exhibited in Fig. 14, revealing that the proposed scheme provides a noticeable load shedding reduction on those islands where the first stage gave a positive value. Please, note that the orange column of the histogram displayed in Fig. 14 stands for the maximum power that could be used on each island as part of the voltage scheme though it has not all been utilised if load shedding is below such value, according to Eq. (42). On the other hand, however, case I considered in Section V of [29] casts only three vulnerable lines (i.e., 7–8, 12–13, and 24–25), resulting in 3 islanded portions. The results of such a comparison are shown in Fig. 15, where the load shedding is zero on the first two islands and non-zero in the third. Despite that load shedding is zero in the first two islands as DERs can feed local loads, it should be stressed that the proposed power regulation scheme would have significantly reduced the load shedding if the second stage had been non-zero.

Finally, the load shedding obtained in both the second and third stages throughout the 24-h evaluation for both Refs. [28,29] is displayed in Fig. 16.

5.2. Comparison with Ref. [34]

In [34], a novel resilience approach for an active distribution network was proposed, which included microgrids and mobile energy units. Although it does not entirely focus on tackling windstorms, it has been selected to underscore the benefits of the proposed scheme when microgrids are co-ordinately deployed to restore the electrical grid when facing large "*N-k*" contingencies. Since Ref. [34] delved into numerous case studies, only Scenario I in Section 4 has been used for comparison purposes, where lines 2–19, 12–13, 9–26, 2–3 and 5–6 were considered vulnerable.

Considering the previously damaged lines and the available resources detailed in Section 4.2, four islands are obtained: island 1 (buses 13 to 18), island 2 (buses 19 through 22), island 3 (23 through 25), and island 4 (buses 26 through 33). In this case, the authors decided to run a 1-h assessment to prove the effectiveness of the proposed scheme, as the capacity of the BESSs was not stated in that paper. The resulting load shedding and voltage profile are provided in Fig. 17 and Fig. 18, respectively. By observing the outcomes displayed in those Figures, it can safely be said that the load shedding has been noticeably reduced in islands 2 and 4 and completely removed in island 1. A crucial insight lies in the low voltage drop across these islands (see Fig. 18), which allows a sufficient voltage margin to be used in the third stage. According to Eq.

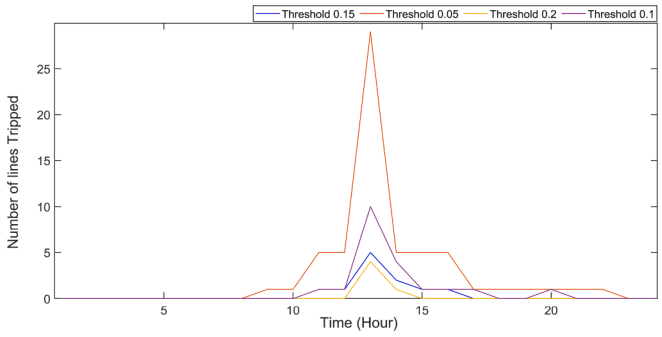

Fig. 11. Representation of the vulnerable lines with different p_{th} over the 24 h period.

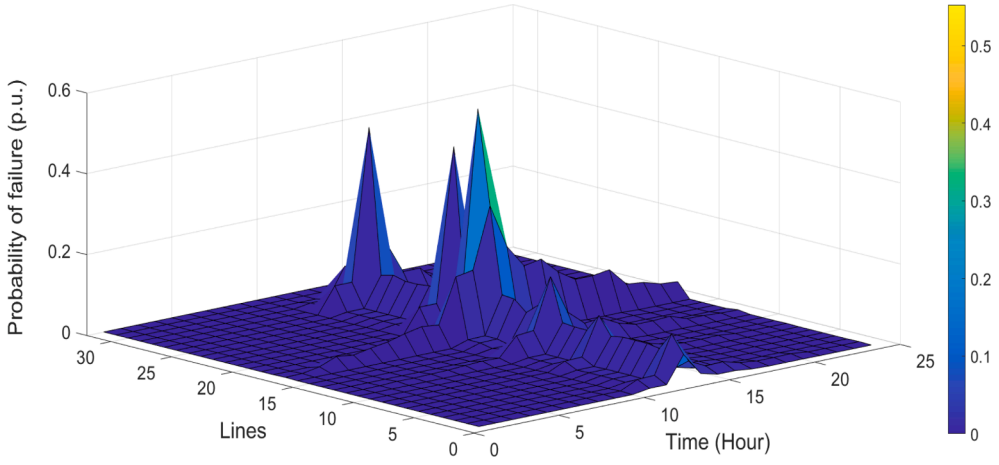

Fig. 10. Graphical representation of the failure probabilities for the sensitivity analysis.

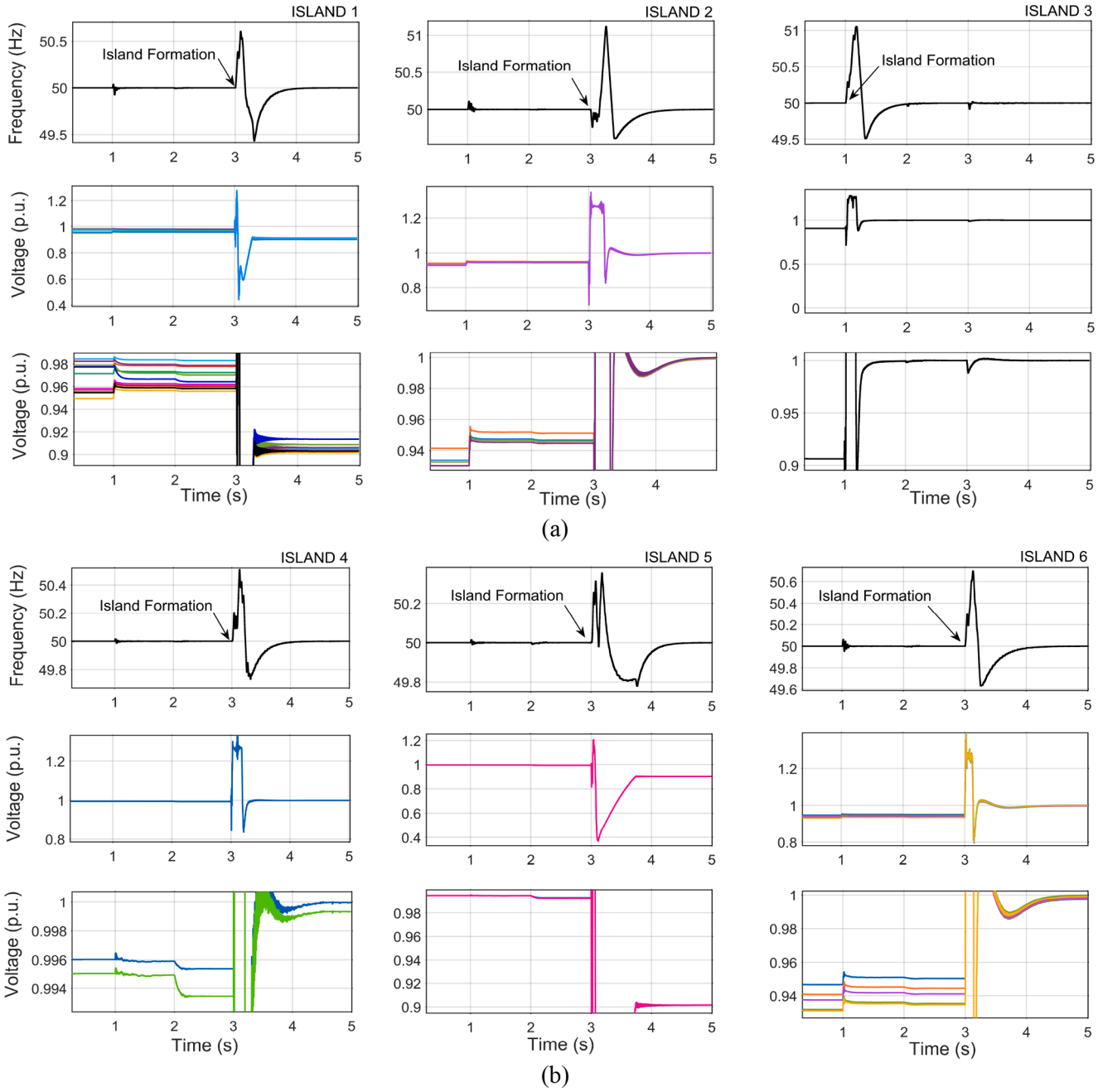

Fig. 12. Results of the time-domain simulations on each island.

Table 5
Detailed parameters of the VSCs used in the time-domain simulations.

Element	Description
Grid-Forming Control Parameters	Frequency droop PI [$K_P = 0.09$; $K_i = 5$]Voltage droop PI [$K_P = 0.1$; $K_i = 7$]Outer loop PI [$K_P = 2$; $K_i = 12$]Inner loop PI [$K_P = 0.3$; $K_i = 20$]Droop gain values [$K_f = 1$ %; $K_V = 4$ %]$f_s = 2.7$ kHz (Switching frequency)$R_f = 0.69$ mΩ; $L_f = 0.18$ mH (RL filter); $Q_f = 10$ kVAr$V_{DC} = 1$ kV; $V_{AC} = 480$ V (rated AC phase-to-phase voltage)
Grid-Following Control Parameters	Active and reactive power controller [$Kp = 10$; $Ki = 15300$]Current PI regulator [$K_P = 0.3$; $K_i = 20$]

(41), more active power could have been taken advantage of to reduce the load shedding without violating the voltage constraints established in the MILP in Eq. (9).

5.3. Comparison with Ref. [49]

Since reference [49] explored the benefits of grid restoration by forming multiple microgrids, it is an appropriate approach for comparison purposes. To provide a feasible comparison with the proposed approach, the IEEE 37 test system used in that paper with the same set of features for both DERs and loads has been reproduced here. As shown in Fig. 5 of [49], the grid is split into three islands where a single dispatchable DERs runs each one. The roots of these islands were allocated in buses 702,728, and 710 with a rated active and reactive power of 252 kW/46 kVAr, 120 kW/171 kVAr and 202/197 kW/171 kVAr, respectively. A one-time slot simulation has been launched to pick up a higher amount of load with respect to the one obtained in [49]. As shown in Fig. 19, a significant amount of load could have been restored on all islands if the proposed approach had been implemented, given the negligible voltage drop across the distribution lines.

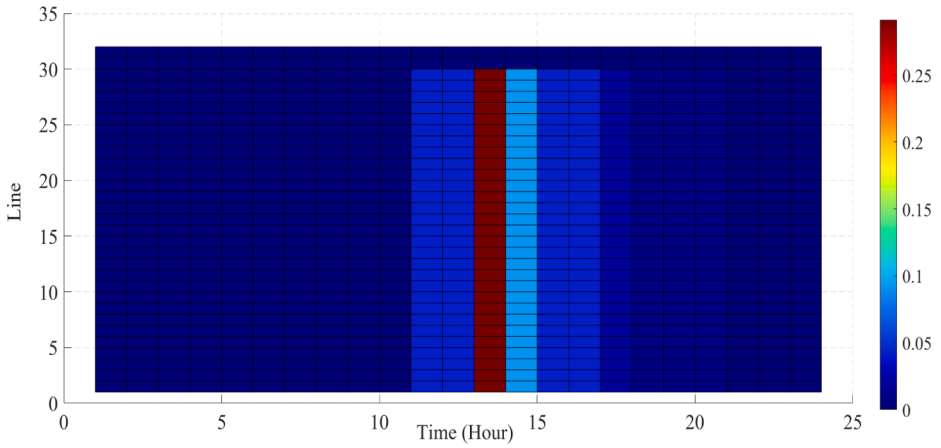

Fig. 13. Failure probabilities with the FCs used in [28].

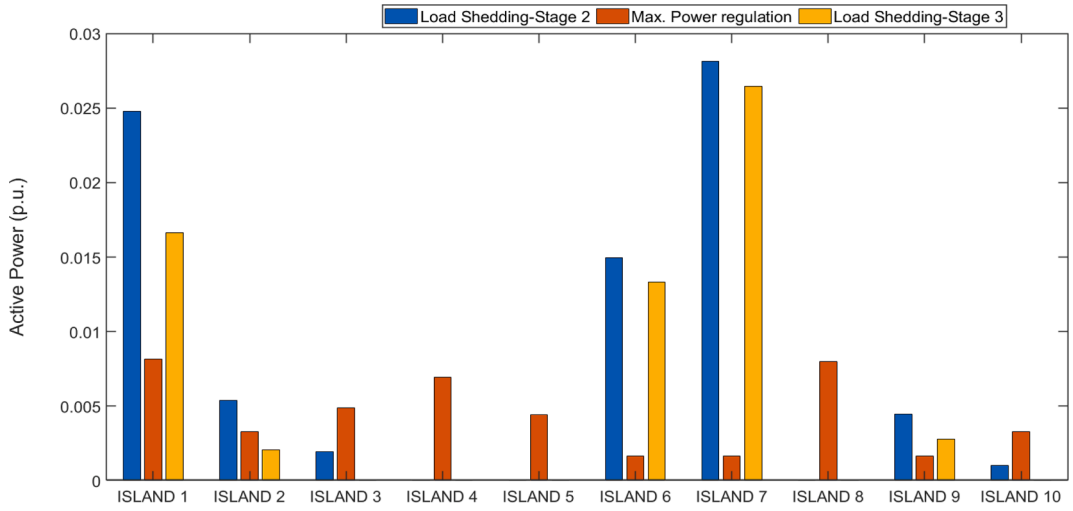

Fig. 14. Comparison with Ref. [28].

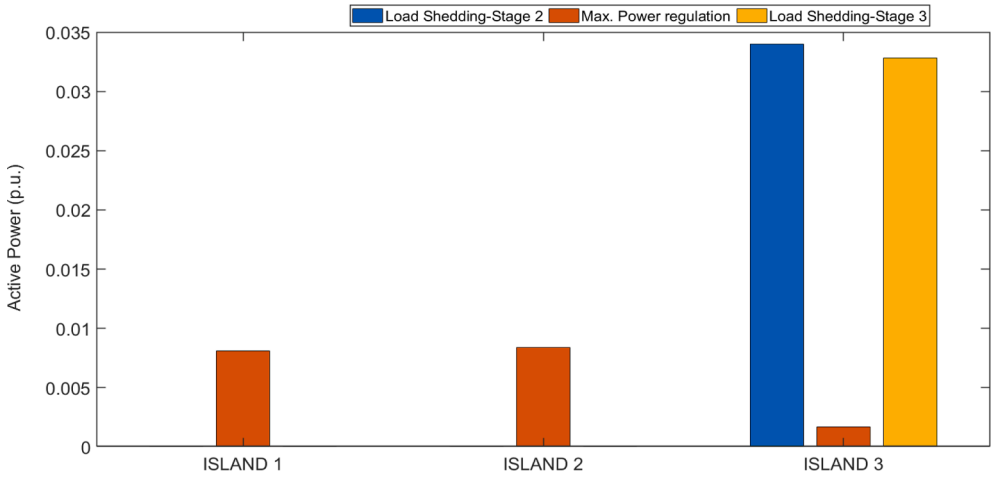

Fig. 15. Comparison with Ref. [29].

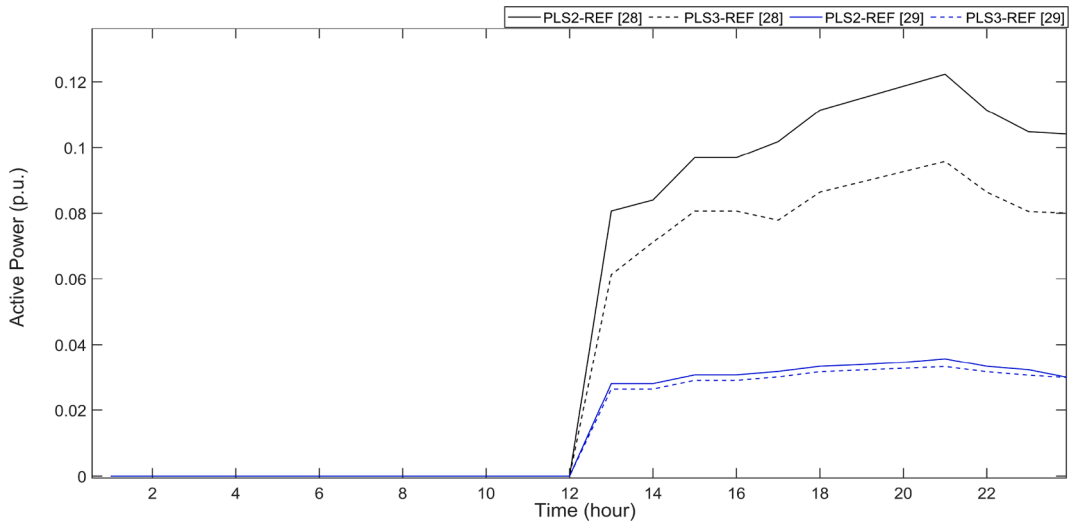

Fig. 16. Load Shedding comparison between [28] and [29].

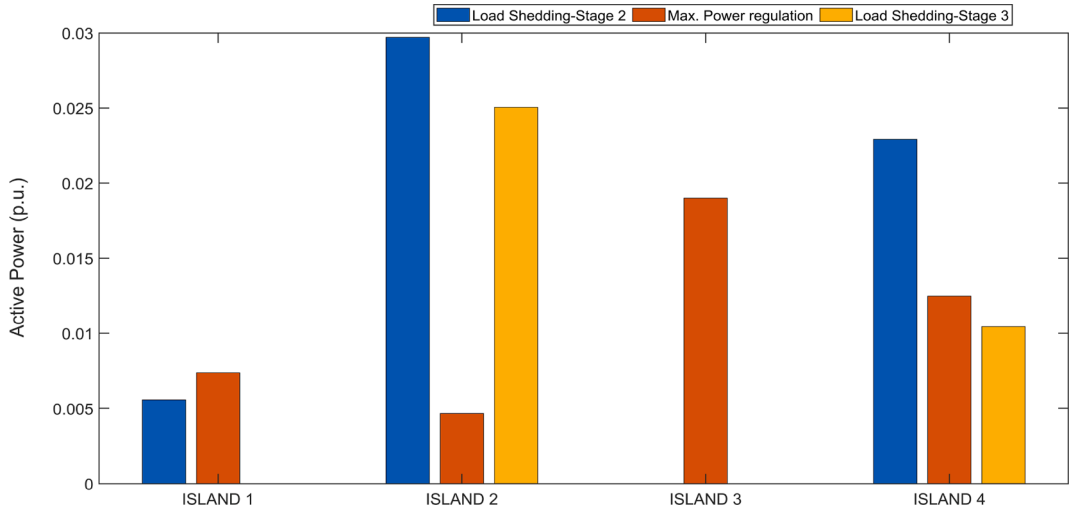

Fig. 17. Comparison results in Section 5.2.

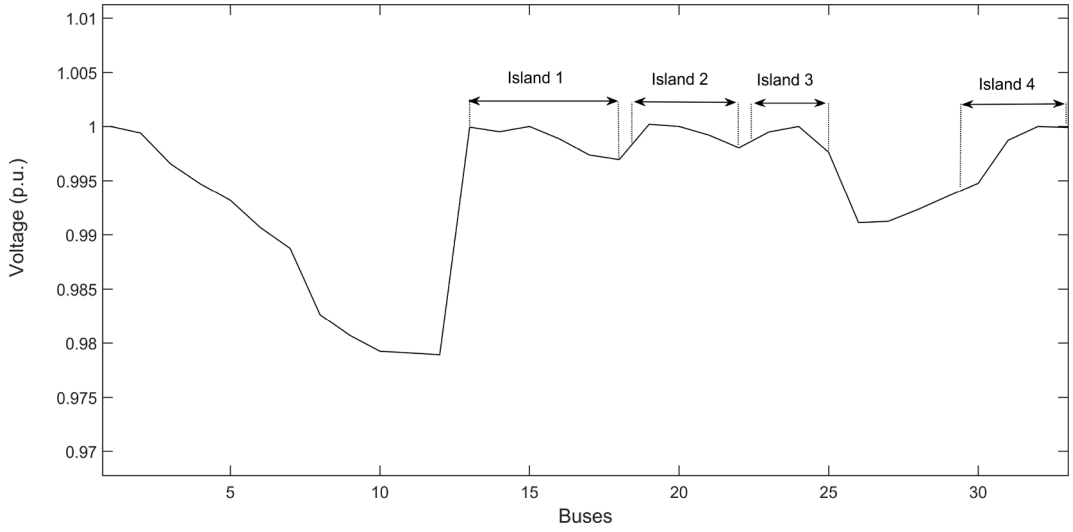

Fig. 18. Voltages obtained in Section 5.2.

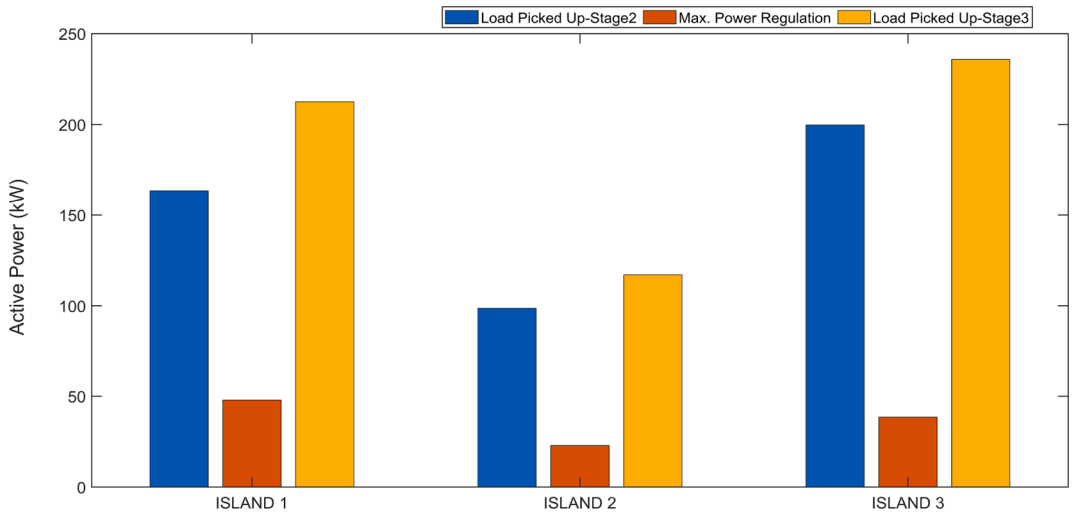

Fig. 19. Comparison with Reference [49].

6. Conclusions

This paper presents a three-stage day-ahead offline resilience assessment to lessen the effects of windstorms in distribution networks by taking advantage of just non-dispatchable DERs and BESSs. The suggested approach has been tested by using a spatiotemporal representation of the 33-bus IEEE test system, where several types of poles and deterioration are included.

The first stage essentially focuses on modelling the vulnerability of the grid assets to calculate the probabilities of failure at each time step throughout the 24-h period given a wind profile retrieved from a meteorological agency. Subsequently, the second stage lies in solving the MILP to split the distribution network into several islands, committing the amount of load to be used as part of a demand-response program and the storage output. Thence, the expected loss of load on each island is obtained. If such a value is larger than zero after the second stage, a novel voltage scheme is used as part of the third stage, where the nature of the DERs and BESSs is used to reduce the load to be shed without violating the voltage constraints imposed in the MILP of the second stage.

In light of the obtained results in Section 4, it has been demonstrated that although there are differences amongst cases, the proposed solution is able to significantly reduce the load shedding whilst keeping voltages within the established limits. Crucially, it has been evidenced that the proposed approach is particularly useful in reducing load shedding if small microgrids scattered along the grid are used in grid restoration, as the voltage drop is negligible in those scenarios. Hence, it becomes a promising solution in grids with a large penetration of DERs with embedded storage systems.

The feasibility of the voltage scheme included in the third stage of the resilience assessment has been validated through time-domain simulations, and the results are included in Section 4.5.

Finally, a remarkable aspect that can be drawn from the comparison in Section 5 is the noticeable impact that the vulnerability model of the grid assets can have in a resilience assessment when windstorms are to be considered.

CRediT authorship contribution statement

Alexandre Serrano-Fontova: Methodology, Software, Conceptualization, Investigation, Writing – original draft. **Zhiyu Liao:** Methodology, Software, Conceptualization, Investigation. **Haiyu Li:** Conceptualization. **Campbell Booth:** .

Declaration of Competing Interest

The authors declare that they have no known competing financial interests or personal relationships that could have appeared to influence the work reported in this paper.

Data availability

No data was used for the research described in the article.

References

[1] "The Physical Science Basis. Contribution of Working Group I to the Sixth Assessment Report of the Intergovernmental Panel on Climate," IPCC, Cambridge, United Kingdom and New York, NY, USA, 2021. [Online]. Available: https://www.ipcc.ch/report/ar6/wg1/downloads/report/IPCC_AR6_WGI_AnnexVI.pdf.
[2] Chaudhary MT, Piracha A. "Natural Disasters—Origins, Impacts, Management," *Encyclopedia,* vol. 1, no. 4, 2021, doi: 10.3390/encyclopedia1040084.
[3] Raoufi H, Vahidinasab V, Mehran K. "Power Systems Resilience Metrics: A Comprehensive Review of Challenges and Outlook," *Sustainability,* vol. 12, no. 22, 2020, doi: 10.3390/su12229698.
[4] Howarth C, Viner D. Integrating adaptation practice in assessments of climate change science: The case of IPCC Working Group II reports. Environ Sci Policy 2022/09/01/ 2022,;135:1–5. https://doi.org/10.1016/j.envsci.2022.04.009.
[5] "The exacerbated effect of storms Dudley, Eunice and Franklin in the UK," in *Ambiental Risk Analytics*, ed. Online, 2022.
[6] Hurricanes Harvey And Irma Show U.S. Must Boost Grid Resiliency. Energy Storage Is Doing Just That." Forbes https://www.forbes.com/sites/energyinnovation/2017/09/08/hurricanes-harvey-and-irma-show-u-s-must-boost-grid-resiliency-energy-storage-is-doing-just-that/?sh=60aeb7a624c9 (accessed).
[7] Busby JW, et al. "Cascading risks: Understanding the 2021 winter blackout in Texas." Energy Res Soc Sci, vol. 77, p. 102106, 2021/07/01/ 2021, doi: https://doi.org/10.1016/j.erss.2021.102106.
[8] "COP26: Together for our planet." United Nations. https://www.un.org/en/climatechange/cop26 (accessed.
[9] (2021). *Net Zero Strategy: Build Back Greener*. [Online] Available: https://assets.publishing.service.gov.uk/government/uploads/system/uploads/attachment_data/file/1033990/net-zero-strategy-beis.pdf.
[10] Ackermann T, Prevost T, Vittal V, Roscoe AJ, Matevosyan J, Miller N. Paving the Way: A Future Without Inertia Is Closer Than You Think. IEEE Power Energ Mag 2017;15(6):61–9. https://doi.org/10.1109/MPE.2017.2729138.
[11] He J, Yuan Z, Yang X, Huang W, Tu Y, Li Y. Reliability Modeling and Evaluation of Urban Multi-Energy Systems: A Review of the State of the Art and Future Challenges. IEEE Access 2020;8:98887–909. https://doi.org/10.1109/access.2020.2996708.
[12] Jufri FH, Widiputra V, Jung J. State-of-the-art review on power grid resilience to extreme weather events: Definitions, frameworks, quantitative assessment methodologies, and enhancement strategies. Appl Energy 2019;239:1049–65. https://doi.org/10.1016/j.apenergy.2019.02.017.
[13] Younesi A, Shayeghi H, Wang Z, Siano P, Mehrizi-Sani A, Safari A. Trends in modern power systems resilience: State-of-the-art review. Renew Sustain Energy Rev 2022/07/01/ 2022,;162:112397. https://doi.org/10.1016/j.rser.2022.112397.

[14] "Building a Resilient UK Energy System," UKERC, 2011. [Online]. Available: https://nora.nerc.ac.uk/id/eprint/16648/1/UKERC_energy_2050_resilience_Res_Report_2011.pdf.
[15] Summary for Policymakers," in *Climate Change The Physical Science Basis: Working Group I Contribution to the Fifth Assessment Report of the Intergovernmental Panel on Climate Change*, C. Intergovernmental Panel on Climate Ed. Cambridge: Cambridge University Press; 2014. p. 1–30.
[16] Hossain E, Roy S, Mohammad N, Nawar N, Dipta DR. Metrics and enhancement strategies for grid resilience and reliability during natural disasters. Appl Energy 2021;290. https://doi.org/10.1016/j.apenergy.2021.116709.
[17] Ma X, Zhou H, Li Z. On the resilience of modern power systems: A complex network perspective. Renew Sustain Energy Rev 2021;152. https://doi.org/10.1016/j.rser.2021.111646.
[18] Chen B, Wang J, Lu X, Chen C, Zhao S. Networked Microgrids for Grid Resilience, Robustness, and Efficiency: A Review. IEEE Trans Smart Grid 2021;12(1):18–32. https://doi.org/10.1109/TSG.2020.3010570.
[19] Shahbazi A, Aghaei J, Pirouzi S, Shafie-khah M, Catalão JPS. Hybrid stochastic/robust optimization model for resilient architecture of distribution networks against extreme weather conditions. Int J Electr Power Energy Syst 2021;126. https://doi.org/10.1016/j.ijepes.2020.106576.
[20] Najafi J, Peiravi A, Guerrero JM. Power distribution system improvement planning under hurricanes based on a new resilience index. Sustain Cities Soc 2018;39:592–604. https://doi.org/10.1016/j.scs.2018.03.022.
[21] Arab A, Khodaei A, Khator SK, Ding K, Emesih VA, Han Z. Stochastic Pre-hurricane Restoration Planning for Electric Power Systems Infrastructure. IEEE Trans Smart Grid 2015;6(2):1046–54. https://doi.org/10.1109/tsg.2015.2388736.
[22] Samani E, Aminifar F. Tri-Level Robust Investment Planning of DERs in Distribution Networks With AC Constraints. IEEE Trans Power Syst 2019;34(5):3749–57. https://doi.org/10.1109/TPWRS.2019.2911576.
[23] Panteli M, Mancarella P, Trakas DN, Kyriakides E, Hatziargyriou ND. Metrics and Quantification of Operational and Infrastructure Resilience in Power Systems. IEEE Trans Power Syst 2017;32(6):4732–42. https://doi.org/10.1109/tpwrs.2017.2664141.
[24] Panteli M, Trakas DN, Mancarella P, Hatziargyriou ND. Power Systems Resilience Assessment: Hardening and Smart Operational Enhancement Strategies. Proc IEEE 2017;105(7):1202–13. https://doi.org/10.1109/jproc.2017.2691357.
[25] Panteli M, Trakas DN, Mancarella P, Hatziargyriou ND. Boosting the Power Grid Resilience to Extreme Weather Events Using Defensive Islanding. IEEE Trans Smart Grid 2016;7(6):2913–22. https://doi.org/10.1109/tsg.2016.2535228.
[26] Moreno R, et al. From Reliability to Resilience: Planning the Grid Against the Extremes. IEEE Power Energ Mag 2020;18(4):41–53. https://doi.org/10.1109/mpe.2020.2985439.
[27] Skarvelis-Kazakos S, et al. Resilience of electric utilities during the COVID-19 pandemic in the framework of the CIGRE definition of Power System Resilience. Int J Electr Power Energy Syst 2022/03/01/ 2022,;136:107703. https://doi.org/10.1016/j.ijepes.2021.107703.
[28] Amirioun MH, Aminifar F, Lesani H. Resilience-Oriented Proactive Management of Microgrids Against Windstorms. IEEE Trans Power Syst 2018;33(4):4275–84. https://doi.org/10.1109/tpwrs.2017.2765600.
[29] Esfahani M, Amjady N, Bagheri B, Hatziargyriou ND. Robust Resiliency-Oriented Operation of Active Distribution Networks Considering Windstorms. IEEE Trans Power Syst 2020;35(5):3481–93. https://doi.org/10.1109/TPWRS.2020.2977405.
[30] Shi Q, et al. Network reconfiguration and distributed energy resource scheduling for improved distribution system resilience. Int J Electr Power Energy Syst 2021;124. https://doi.org/10.1016/j.ijepes.2020.106355.
[31] Postigo Marcos F, Mateo Domingo C, Gómez San Román T. "Improving distribution network resilience through automation, distributed energy resources, and undergrounding," *Int J Elect Power Energy Systems,* vol. 141, 2022, doi: 10.1016/j.ijepes.2022.108116.
[32] Skarvelis-Kazakos S, et al. Resilience of electric utilities during the COVID-19 pandemic in the framework of the CIGRE definition of Power System Resilience. Int J Electr Power Energy Syst 2022;136. https://doi.org/10.1016/j.ijepes.2021.107703.
[33] Roofegari nejad R, Sun W, Golshani A. "Distributed Restoration for Integrated Transmission and Distribution Systems With DERs," *IEEE Trans Power Syst,* vol. 34, no. 6, pp. 4964-4973, 2019, doi: 10.1109/tpwrs.2019.2920123.
[34] Mishra DK, Ghadi MJ, Li L, Zhang J, Hossain MJ. Active distribution system resilience quantification and enhancement through multi-microgrid and mobile energy storage. Appl Energy 2022;311. https://doi.org/10.1016/j.apenergy.2022.118665.
[35] Gautam P, Piya P, Karki R. Resilience Assessment of Distribution Systems Integrated With Distributed Energy Resources. IEEE Trans Sustain Energy 2021;12(1):338–48. https://doi.org/10.1109/tste.2020.2994174.
[36] Najafi Tari A, Sepasian MS, Tourandaz Kenari M. "Resilience assessment and improvement of distribution networks against extreme weather events," *Int J Elect Power Energy Syst,* vol. 125, 2021, doi: 10.1016/j.ijepes.2020.106414.
[37] Ceferino L, Lin N, Xi D. Stochastic modeling of solar irradiance during hurricanes. Stoch Env Res Risk A 2022/01/10 2022,. https://doi.org/10.1007/s00477-021-02154-2.
[38] Mohammadi Darestani Y, Shafieezadeh A. Multi-dimensional wind fragility functions for wood utility poles. Eng Struct 2019;183:937–48. https://doi.org/10.1016/j.engstruct.2019.01.048.
[39] Dunn S, Wilkinson S, Alderson D, Fowler H, Galasso C. Fragility Curves for Assessing the Resilience of Electricity Networks Constructed from an Extensive Fault Database. nat Hazard Rev 2018/02/01 2018,;19(1):04017019. https://doi.org/10.1061/(ASCE)NH.1527-6996.0000267.
[40] Salman AM, Li Y. Age-dependent fragility and life-cycle cost analysis of wood and steel power distribution poles subjected to hurricanes. Struct Infrastruct Eng 2016/08/02 2016,;12(8):890–903. https://doi.org/10.1080/15732479.2015.1053949.
[41] Shafieezadeh A, Onyewuchi UP, Begovic MM, DesRoches R. Age-Dependent Fragility Models of Utility Wood Poles in Power Distribution Networks Against Extreme Wind Hazards. IEEE Trans Power Delivery 2014;29(1):131–9. https://doi.org/10.1109/TPWRD.2013.2281265.
[42] Teoh YE, Alipour A, Cancelli A. Probabilistic performance assessment of power distribution infrastructure under wind events. Eng Struct 2019/10/15/ 2019,;197:109199. https://doi.org/10.1016/j.engstruct.2019.05.041.
[43] Salman AM, Li Y. Age-dependent fragility and life-cycle cost analysis of wood and steel power distribution poles subjected to hurricanes. Struct Infrastruct Eng 2015;12(8):890–903. https://doi.org/10.1080/15732479.2015.1053949.
[44] Lee S, Ham Y. Probabilistic framework for assessing the vulnerability of power distribution infrastructures under extreme wind conditions. Sustain Cities Soc 2021;65. https://doi.org/10.1016/j.scs.2020.102587.
[45] Noebels M, Preece R, Panteli M. A machine learning approach for real-time selection of preventive actions improving power network resilience. IET Gener Transm Distrib 2021;16(1):181–92. https://doi.org/10.1049/gtd2.12287.
[46] Panteli M, Pickering C, Wilkinson S, Dawson R, Mancarella P. Power System Resilience to Extreme Weather: Fragility Modeling, Probabilistic Impact Assessment, and Adaptation Measures. IEEE Trans Power Syst 2017;32(5):3747–57. https://doi.org/10.1109/tpwrs.2016.2641463.
[47] Murray K, Bell KRW. "Wind related faults on the GB transmission network," in: *2014 International Conference on Probabilistic Methods Applied to Power Systems (PMAPS)*, 7-10 July 2014 2014, pp. 1-6, doi: 10.1109/PMAPS.2014.6960641.
[48] E. C. f. M.-R. W. Forecasts. "Climate Data Store." https://cds.climate.copernicus.eu/#!/home (accessed).
[49] Ding T, Lin Y, Li G, Bie Z. A New Model for Resilient Distribution Systems by Microgrids Formation. IEEE Trans Power Syst 2017;32(5):4145–7. https://doi.org/10.1109/tpwrs.2017.2650779.
[50] Schimtz S. Aerodynamics of Wind Turbines: A Physical Basis for Analysis and Design. Wiley, 2019, p. 334.
[51] Ghamrawi A, Gaubert J-P, Mehdi D. A new dual-mode maximum power point tracking algorithm based on the Perturb and Observe algorithm used on solar energy system. Sol Energy 2018/11/01/ 2018,;174:508–14. https://doi.org/10.1016/j.solener.2018.09.013.
[52] Bakhshi-Jafarabadi R, Sadeh J, Serrano-Fontova A, Rakhshani E. "Review on islanding detection methods for grid-connected photovoltaic systems, existing limitations and future insights," *IET Renew Power Generation,* https://doi.org/10.1049/rpg2.12554 vol. n/a, no. n/a, 2022/07/20 2022, doi: https://doi.org/10.1049/rpg2.12554.
[53] A. Serrano-Fontova, J. A. Martinez, P. Casals-Torrens, and R. Bosch, "A robust islanding detection method with zero-non-detection zone for distribution systems with DG," in *International Journal of Electrical Power & Energy Systems* vol. 133, ed: Elsevier, 2021, p. 107247.
[54] UK U. C. Met Office. "Red Weather Warning issued for Storm Eunice. https://www.metoffice.gov.uk/about-us/press-office/news/weather-and-climate/2022/red-weather-warning-issued-for-storm-eunice (accessed).
[55] Li Y, Gu Y, Green T. "Revisiting Grid-Forming and Grid-Following Inverters: A Duality Theory," *IEEE Trans Power Sys,* pp. 1-1, 2022, doi: 10.1109/TPWRS.2022.3151851.
[56] Sonal et al and D. Gosh, "Hybrid data–driven resilience assessment and enhancement of distribution system for cyclone susceptible zones," *Scientific Reports Nature portfolio,12,* pp. 9492 (2022) doi: 10.1038/s41598-022-13311-0.